2004

Near infrared surface plasmon resonance spectroscopy : theoretical studies

Michelle Nga Doan
San Jose State University

NEAR INFRARED SURFACE PLASMON RESONANCE SPECTROSCOPY: THEORETICAL STUDIES

A Thesis

Presented to

The Faculty of the Department of Chemistry

San Jose State University

In Partial Fulfillment

of the Requirements for the Degree

Master of Science

By

Michelle Nga Doan

December 2004

APPROVED FOR THE DEPARTMENT OF CHEMISTRY

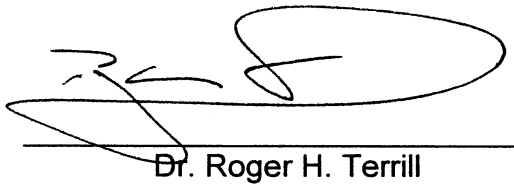

Dr. Roger H. Terrill

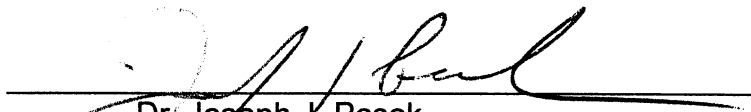

Dr. Joseph J. Pesek

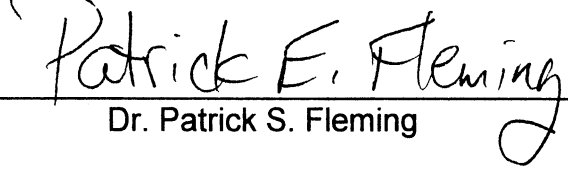

Dr. Patrick S. Fleming

APPROVED FOR THE UNIVERSITY

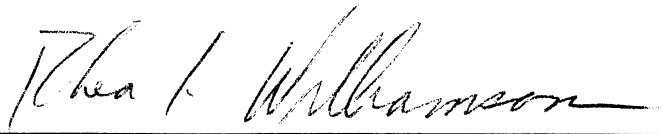

ABSTRACT

NEAR INFARED PLASMON RESONANCE SPECTROSCOPY: THEORETICAL STUDIES

By Michelle Nga Doan

Surface plasmon resonance spectroscopy (SPRS) is a sensitive optical method of analysis that can be used to measure thin films adsorbed onto thin Au or Ag films coated onto an optical substrate and under a specific set of conditions. Although the SPRS method is quite sensitive, its application requires additional means for qualitatively determining the nature of the adsorbed material (analyte). Toward this end it is helpful to correlate ordinary absorption spectra with the reflected light spectrum of the adsorbed substance when the reflections are occurring under conditions that excite a surface plasmon resonance. This is accomplished in theory using the Kramers-Kronig transformation (KKT) to compute the requisite optical constants of the absorbers and Fresnel numerical simulations of the wavelength and angle dependent reflectivity – so called SPR curves. Calculations reveal that the spectral fingerprint of the adsorbate is present in the SPR-coupled reflection data.

ACKNOWLEDGEMENTS

I am grateful for the support of my research advisor, thesis committee, and my family without whom I could not achieve my goal.

I am especially indebted to Dr. Roger Terrill, my research advisor, for his patience and understanding. He was gracious to take me in when my original research advisor left SJSU. His guidance and encouragement have been invaluable.

Dr. Pesek and Dr. Fleming, my research committee, have graciously spent time attending my seminars and oral exams as well as correcting my thesis.

TABLE OF CONTENTS

LIST OF FIGURES

1. INTRODUCTION

1.1 Overview of Surface Plasmon Resonance (SPR)

A surface plasmon (SP) is a collective oscillation of electron density that propagates along the surface of a metal. In the correct configuration, light can be used to excite a surface plasmon. For example, light, of a specific wavelength and at a specific angle, internally reflected from the interface between glass and a 50 nm Ag film can excite a surface plasmon in the Ag film. The evanescent electromagnetic field of the SP extends out from the surface of the Ag film into the medium opposite the glass substrate. The electric field intensity of the SP is concentrated at the outer surface of the metal film and decreases exponentially away from the metal-dielectric interface. The medium contacting the Ag film profoundly affects the SP, so surface plasmon resonance (SPR) spectroscopy can be used as a sensitive chemical sensor that probes only a few hundred nanometers from the metal surface.

When the light wave vector matches that of the surface plasmon, energy is transferred from photons to plasmons – this occurs under *resonance conditions*. The SP resonance excitation can be observed as a sharp minimum of the reflectance as a function of angle (for monochromatic light) or as a function of wavelength (for white light at a fixed angle). The position of the absorption band (θ_{SPR} or λ_{SPR}) is a highly sensitive function of the refractive index (RI) of the phase contacting the external surface of the metal film.

SPR spectroscopy has emerged as a powerful tool to monitor adsorption phenomena at an interface in real time. During the past decade, the SPR technique has developed significantly. With detection limits of SPRS measurements to changes as little as 10^{-7} RI units [1,2,3], SPRS can easily detect sub-nanogram quantities of diffusing analytes when they interact with a surface bound host. Its main applications deal with studies of biomolecular interactions, monitoring the molecular assembly process, and studies of protein conformation change. The SPR response is quasi-linear and can be acquired in real-time, so measurements of SPRS can yield both thermodynamic and kinetic information on a given host-guest (e.g. enzyme-substrate) interaction. SPRS can extend to the electrochemical field where an electrochemical process such as the adsorption of species, the modification of an electrode surface, etc., perturbs the excitation of surface plasmons [4].

1.2 Research objective

SPRS has great sensitivity but, the way it is typically implemented, it lacks selectivity. The typical SPRS signal, i.e. a shift in the coupling wavelength ($\Delta\lambda_{SPR}$) or angle ($\Delta\theta_{SPR}$), does not distinguish between the appearance of the analyte and that of interfering adsorbates. So, the selectivity of such an SPRS measurement depends entirely on the selectivity of the surface chemistry – for example the selectivity of a given surface-bound antibody 'probe' to its diffusing antigen 'target'. Similarly, it is impossible to determine more than one parameter from a one-dimensional shift such as $\Delta\lambda_{SPR}$ or $\Delta\theta_{SPR}$. For example, the thickness

(d) of an adsorbate layer can be calculated if its refractive index (n) is known or *vice-versa*. In order to gain selectivity, SPR detection is often coupled with a second analytical method. Ex-situ approaches such as matrix assisted laser desorption-ionization spectrometry (MALDI-MS) [5], ellipsometry [6], and Raman spectroscopy [7] have been used in tandem with SPRS to obtain selective information of the absorbates.

In this study, the spectral selectivity limitation of SPRS is evaluated by calculating reflectivity data as a function of both wavelength and angle. In this way, a qualitative spectral fingerprint can be obtained for a given *absorbing* analyte. The 'fingerprint' derives from and resembles the optical constants of the near-surface absorber – i.e. the complex refractive index $N(\lambda)$, where $N(\lambda) = n(\lambda) + ik(\lambda)$, $n(\lambda)$ being the real and $k(\lambda)$ the imaginary part of the refractive index (RI). The optical constant '$k(\lambda)$' is a manifestation of the extinction coefficient $\alpha(\lambda)$ (cm^{-1}) (or the molar extinction $\varepsilon(\lambda)$ ($\mathbf{M}^{-1}cm^{-1}$)). In this work, literature absorption spectra are used to compute $k(\lambda)$, and $k(\lambda)$ is then transformed into $n(\lambda)$ via the Kramers-Kronig transformation (KKT) [8]. The resulting $N(\lambda)$ data are then used to compute the full reflectivity surface ($R(\lambda,\theta)$) using the Fresnel equations. The $R(\lambda,\theta)$ calculation reveals a curved, roughly diagonal trajectory of the surface plasmon in the wavelength-angle plane. In the presence of an absorbing species that interacts with the surface plasmon, interesting coupling can be observed that yields a spectral fingerprint of the near surface absorber that clearly reflects $N(\lambda)$.

Most analytes of interest do not posses absorption bands in the visible wavelength region, so SPR will not be significantly selective in this region. Nor is SPR possible in the ultraviolet because of the unfavorable optical properties of the relevant metals in this range. However, the optical constants of both Au and Ag in the *near infrared* (NIR) region are amenable to SPR measurements and nearly all molecules exhibit unique vibrational overtone spectra in this frequency range. Hence, these simulations focus on NIR SPR spectra of a simple model compound, isoamyl alcohol, for which absorbance spectra are available.

2. THEORY

2.1 SPR theory

Surface plasmons are charge density waves that oscillate along the surface of a metal. Under conditions of total internal reflection, when light strikes an interface between e.g. glass and a 50nm Au or Ag metal film, part of the incident energy can interact with the delocalized surface plasmon wave (SPW) The SPW is excited in the metal and has a maximum in electric field strength at the surface of the metal opposite the incident light – i.e., on the outer surface of the metal film. The surface plasmon resonance effect is observed as the loss of reflected light energy and it results in a sharp attenuation of reflectivity. The resonance condition depends on the wavelength and the angle of incidence of the light, and the dielectric constants of all the involved materials. The resonant angles and wavelengths are extremely sensitive to the refractive index (or

complex dielectric constant) of the material in contact with the metal surface of the SPR sensor. For sensor applications, shifts in the wavelength or the angle of minimum reflectivity characterize changes in the refractive index of the material in contact with the metal surface of the SPR sensor. Only transverse magnetically polarized light (the electric field polarized in the plane of incidence) may couple to surface plasmons.

2.2 SPR configuration

2.2.1 Total Internal Reflection (TIR)

An unpolarized beam of light comprises countless superposed propagating EM waves, the electric field vectors of each randomly oriented around the direction of propagation. In a polarized beam the E-field intensity is limited to a single plane. This is relevant to the discussion of how light E-fields interact with surfaces in SPRS – a reflection experiment. For polarized light reflecting off of a surface, the E-field vector may fall in the plane of incidence (p-polarized transverse magnetic (TM)) or perpendicular to it (s-polarized or transverse electric (TE), as illustrated in Figure 1.

When light is incident at an interface, it is split into the refracted wave and reflected wave. By the law of reflection, the angle of incidence equals the angle of reflection. When the wave passes from one non-absorbing medium n_1 to another n_2, the angle of incidence θ_i and the angle of refraction θ_t with respect to the normal to the interface, are related by:

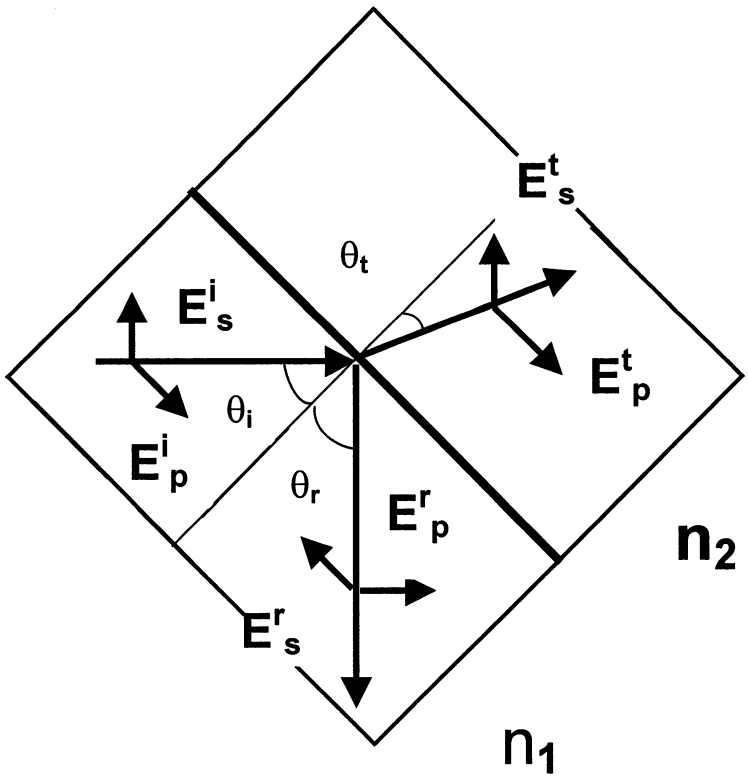

Figure 1: p-polarized and s-polarized waves. E is the electric vector, θ is the angle and n is the refractive index; the superscripts i, t and r denote incidence, transmission and refraction respectively; the subscripts s and p denote s-polarized wave and p-polarized wave respectively.

$$n_1 \cdot \sin(\theta_i) = n_2 \cdot \sin(\theta_t) \quad (1)$$

or $$\frac{\sin(\theta_i)}{\sin(\theta_t)} = \frac{n_2}{n_1} = cons\tan t \quad (2)$$

This relationship is Snell's law of refraction: light bends away from the normal when it travels from an optically denser medium into an optically less dense medium, and vice versa.

When the angle of refraction θ_t equals 90^0, the angle of incidence is known as the critical angle:

$$\theta_{crit} = \theta_i = \arcsin(\frac{n_1}{n_2}) \quad (3)$$

When light is incident through a transparent substrate such as a prism where the incident angle is greater or equal to the critical angle, all the incoming energy of the radiation from the high refractive index medium to a low refractive one is reflected back into the incident medium. This phenomenon is called total internal reflection (Figure 2).

2.2.2 SPR dispersion curve

Under total internal reflection, the optical E-field along the direction of propagation, E_X, has the usual oscillation character but the E_Z component perpendicular to the interface, penetrates the interface and decays exponentially with a decay length, l, which is a function of the incident angle. This E_Z electromagnetic field distribution is called an evanescent wave. Qualitatively, it is the E_Z evanescent field that excites the SP.

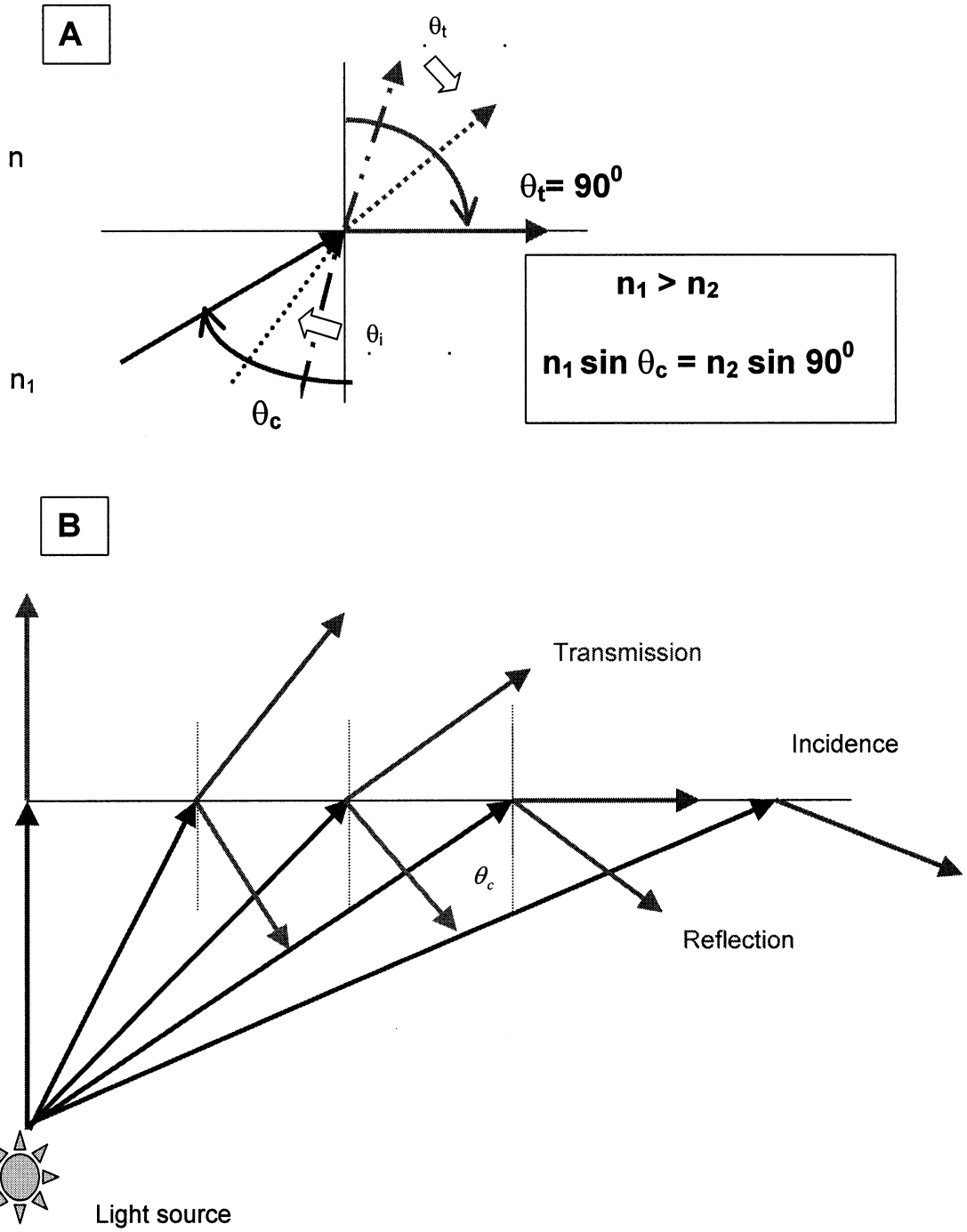

Figure 2:Total Internal Reflection

A. If $\theta_i = \theta_{crit}$, $\theta_t = 90^0$. B. The light incidence at an interface splits into reflected wave and transmitted wave. When $\theta_i > \theta_{crit}$, all the incident energy is reflected back to the incident medium.

SPR occurs when the momentum of the incident light matches that of the surface plasmon wave (SPW). The momenta of the SPW and the incident light are given by their respective wave vectors K_{SPR} and K_X. For the excitation of surface plasmons, only the photon wave vector projection along the x-direction is relevant because plasmons are confined to the plane of the metal film. The propagation of an electromagnetic wave through a medium is governed by the complex refractive index of the medium $N(\omega) = n(\omega) + ik(\omega)$ where $n(\omega)$ and $k(\omega)$ are real functions of frequency ω.

The wave vector of photons, K_{PH}, propagating in the dielectric medium is always smaller than that of the SPW, K_{SPR}, propagating at an interface between the same medium and the metal (Figure 3A)[9]:

$$K_{PH} = \frac{\omega}{c} \cdot \sqrt{\varepsilon d} \qquad (4)$$

where c is the speed of light in vacuum and ε_d is the dielectric constant in the dielectric medium.

The dispersion of photons in the dielectric medium is described by the 'light line':

$$\omega = K_{PH} \cdot c_d \qquad (5)$$

with the speed of light in the dielectric medium, $c_d = \frac{c}{\sqrt{\varepsilon_d}}$.

To vary K_X along metal/dielectric (i.e. outer) interface, one can tune the angle of incidence θ from zero at normal incidence (point O, Figure 3B) to the full

wave vector K_{PH} at grazing incidence (point A, Figure 3B). But this is not enough to satisfy the resonance condition of the SPW – the SPW dispersion curve lies to the right side of the dispersion of photon in the dielectric medium. Hence, the coupling is achieved using an internal reflection method (curve C, Figure 3B) as discussed below.

2.2.3 SPR in the Kretschmann or Attenuated Total Reflection (ATR) configuration

Kretschmann [10] and Otto [11] demonstrated that optical excitation of surface plasmons could be obtained by the method of attenuated total reflection (ATR). In this method, light is coupled to the interface via the evanescent wave that exists when light is totally internal reflected at the base of the high index prism (with $\varepsilon_p > \varepsilon_d$). There are two variants of this ATR method. In the first, less commonly used one, dubbed the Otto-configuration, the base of a high index prism is stationed within a few tens of nm from the surface of a metal. Photons are coupled into the SPW mode of the metal surface via the evanescent tail of light totally internally reflected at the base of the high-index prism. By tuning the angle of incidence, resonant coupling between evanescent photons and surface plasmons can be obtained (point B, Figure 3B). The technical draw backs of this configuration are firstly that the gap between the prism base and the metal surface must be so small that coupling is difficult (typically set by adventitious dust particles) and secondly that the active (sensing) surface is effectively trapped between the prism and the metal where analytes are hard to introduce.

Kretschmann and Raether introduced a more convenient coupling configuration. In the Kretschmann configuration, light is internally reflected from the interface between a high index prism and a *thin* (50 nm typically) metal layer that is evaporated directly onto the base of the prism. In this way, the K_X value is set by the high index prism, but couples to the metal dielectric interface via an evanescent field. The resonant coupling between the evanescent field and the SPW is observed as a function of the angle of incidence or wavelength. A sharp minimum in the reflectivity spectrum $R(\lambda)$ or $R(\theta)$ occurs when surface plasmons are excited (Figure 4). Surface plasmon resonance spectroscopy (SPRS) is usually done in the experimental configuration introduced by Kretschmann and Rather (Figure 5). A thin metal layer is vacuum deposited directly onto the base of the prism or the onto a glass slide which is then index-matched to the base of the prism. The evanescent field of a photon can then excite the plasmons in the thin metal layer. Maxwell's equations describe the SPW. The SPW is a bound wave that propagates along the interface, with a wave vector (K_{SPR}) given as:

$$K_{SPR} = K_0 \cdot \sqrt{\frac{(\varepsilon_M \cdot \varepsilon_D)}{(\varepsilon_M + \varepsilon_D)}} \qquad (6)$$

where ε_M and ε_D are the complex dielectric constants of the metal and dielectric layer, and the free space wave vector $K_0 = 2\pi / \lambda$. The complex dielectric constant is related to wavelength-dependent refractive index by:

$$\varepsilon(\lambda) = \varepsilon'(\lambda) + i \cdot \varepsilon''(\lambda) = N(\lambda)^2 = (n'(\lambda) + i \cdot k''(\lambda))^2 \qquad (7)$$

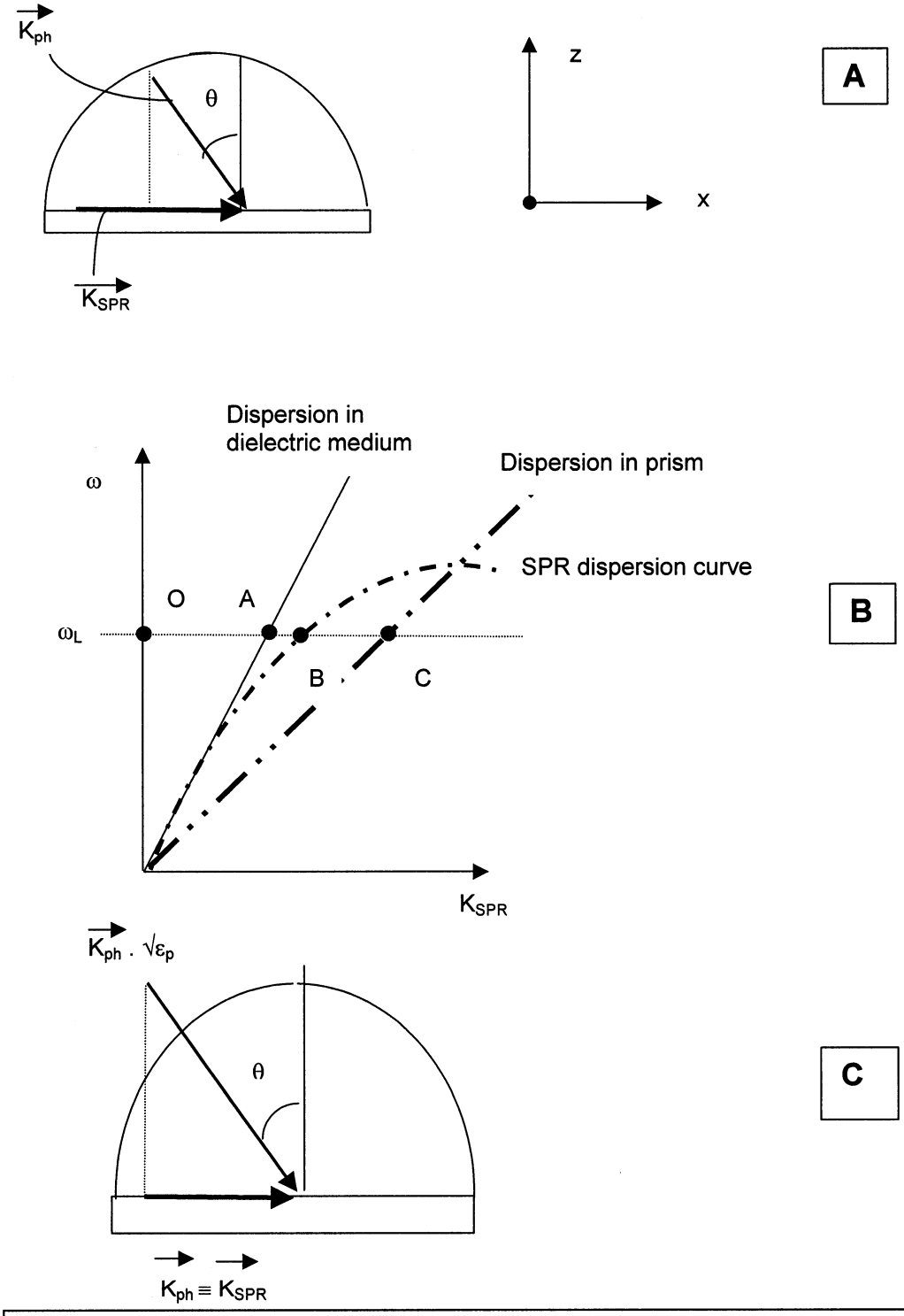

Figure 3: Dispersion curves. A. Momentum relation between a surface plasmon wave vector, K_{SPR} and a photon incident wave vector, K_{ph} at the interface at an angle, θ. B. Dispersion relation of a photon traveling in the dielectric medium and of a proton propagating in the prism. C. Wave vector matching condition for the surface plasmon resonance: $K_{ph} \equiv K_{SPR}$.

where ε_M and ε_D are the complex dielectric constants of the metal and dielectric layer, and the free space wave vector $K_0 = 2\pi / \lambda$. The complex dielectric constant is related to wavelength-dependent refractive index by

$$\varepsilon(\lambda) = \varepsilon'(\lambda) + i \cdot \varepsilon''(\lambda) = N(\lambda)^2 = (n'(\lambda) + i \cdot k''(\lambda))^2 \quad (7)$$

Light incident to the interface at an angle normal to θ_i has a wave vector, K_x,

$$K_x = K_0 \cdot n_i \cdot \sin(\theta_i) \quad (8)$$

If the wave vector of the evanescent wave, K_x, equals that of the SPW, denoted as K_{SPR}, then the resonant conditions are satisfied and the energy is transferred from photons to the surface plasmons.

Whenever there is a change in the refractive index of the sample on the sensor area, a shift in the spectral location of the SP resonance will be observed. This shift is the basis of SPR sensors and is illustrated in Figure 4.

2.3 Real and imaginary parts of refractive index

2.3.1 Complex refractive index

When light travels from, e.g. air to a non-absorbing material such as glass, diamond, or plastic, it is refracted (bent) at the interface. The change in speed of light through a medium is expressed through the refractive index n:

$$n = \frac{c}{v} \quad (9)$$

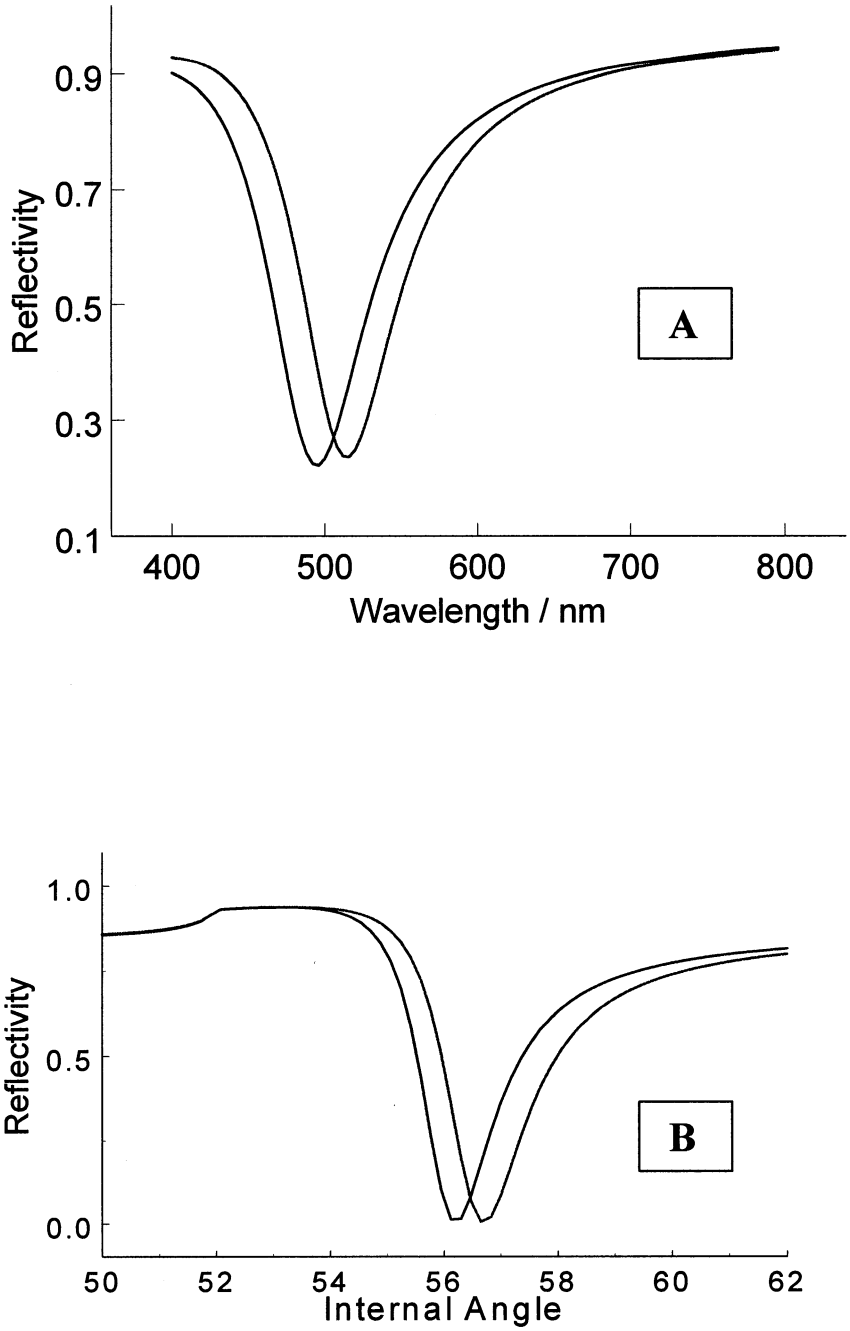

Figure 4: SPR reflectivity curves.

A. SPR reflectivity as a function of wavelength. B. SPR reflectivity as a function of angle. Blue and red curves correspond to clean metal, and metal coated with a 20 nm layer of material with refractive index 1.4.

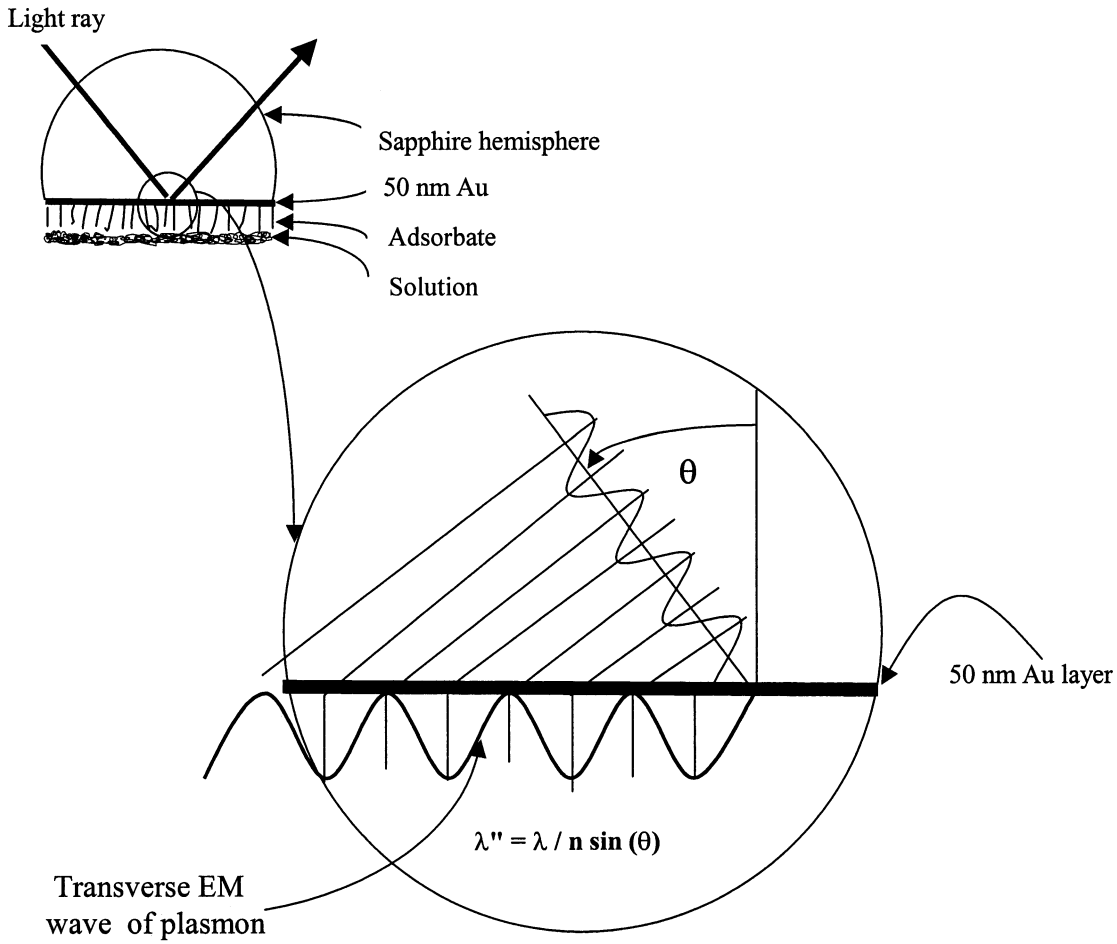

Figure 5: 4-layer Kretschmann configuration. Upper left figure shows optic with Au film and solution layers. Expanded view of interface depicts the interaction of the electric field component of incidence at angle theta. At the right incident angle theta, the photon projection along the x-coordinate, K^{x}_{ph}, matches the wave vector K_{SPR}.

where n, c and ν are the refractive index, the speed of light in vacuum, and the speed of light in a given material respectively. A complex refractive index N is defined when light passes through materials that absorb as well as refract as:

$$N = n + ik \tag{10}$$

N consists of a real part, n describing the refraction, and of an imaginary part, k describing the absorption of the materials. Both parts are dependent on the wavelength of light, and this dependence is known as dispersion.

$$N(\lambda) = n(\lambda) + ik(\lambda) \tag{11}$$

2.3.2 Kramers-Kronig transformation (KKT)

The Kramers-Kronig transformation (KKT) can be employed to interconvert n(v) and k(v). This is important because k(v) is accessible experimentally through absorbance spectra, but n(v) is not, and both are needed to simulate the reflectivity. The KKT is equivalent to the Hilbert transformation [12]. The KKT is based on the principle of causality when the time interval between cause and effect is positive. The KKT describes the interrelationships between the real and imaginary components of a function in the complex plane. The KK transforms of n and k are:

$$n(\upsilon_i) - n(\infty) = \frac{1}{\pi} \cdot P \int_{-\infty}^{\infty} \frac{k(\upsilon)}{\upsilon - \upsilon_i} d\upsilon \tag{12}$$

$$k(\nu_i) = -\frac{1}{\pi} \cdot P \int_{-\infty}^{\infty} \frac{n(\nu) - n(\infty)}{\nu - \nu_i} d\nu \tag{13}$$

The KKT is often used to derive either the real or the imaginary parts of the refractive index function when the other part is known. In this case, the k(ν) spectrum is computed from a literature absorbance spectrum, and n(ν) is derived from a KKT of k(ν). Instead of implementing the direct numerical integration described above, we use a fast Fourier transform (FFT) algorithm described for this purpose by Bertie et al [8]. The FFT algorithm is known as the Hilbert transformation and is simply the result of two serial FFT operations. The equivalency between the Hilbert transformation and the successive double Fourier transformation is well known. The interrelationship between n(λ) and k(λ) spectra are illustrated in Figure 6 [13]. In this case, the k(λ) spectrum is derived from the absorbance spectrum, made in our laboratory, of magnesium phthalocyanine. The k(λ) spectrum directly reflects the absorption band whereas the n(λ) closely resembles the derivative of k(λ).

2.3.3 The wave equation in a damping medium

If Maxwell's equations are applied to EM radiation under the assumptions that there are no free charges, no currents, and all materials are non-magnetic, then both electric field E and magnetic field B are perpendicular to the direction of the propagation of the wave and they are also perpendicular to each other [14]. Consider a plane wave propagating in the positive z direction with a frequency ω and a wave vector K. The x-component of the electric field vector E has the form:

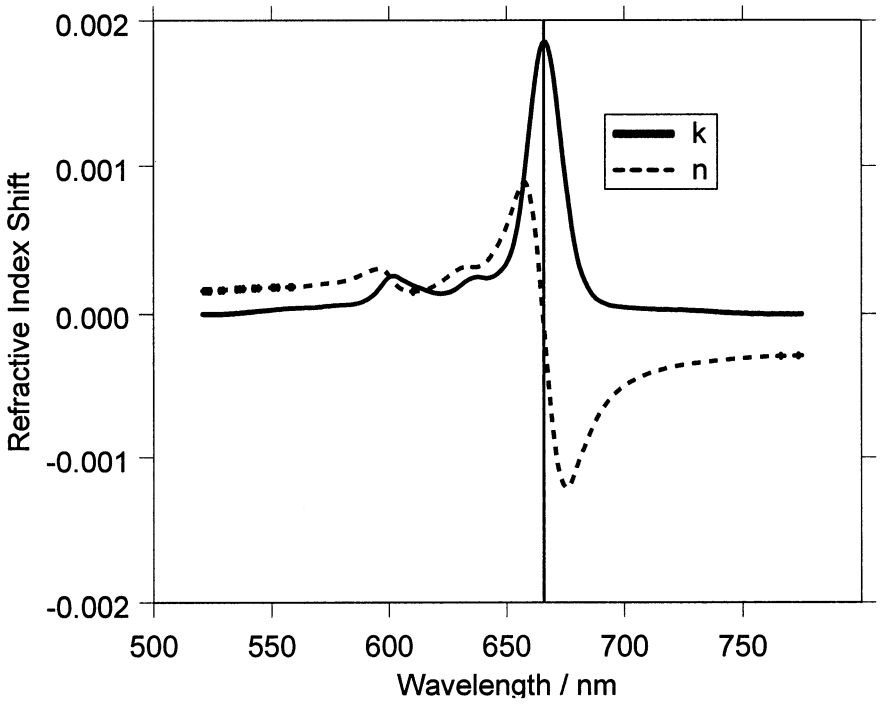

Figure 6: Refractive index spectrum, n(λ) and absorbance spectrum, k (λ).

$$E_x = E_0 \cdot e^{i(\omega t - Kz)} \tag{14}$$

with the angular frequency, ω

$$\omega = \frac{c \cdot k}{\sqrt{\varepsilon}} \tag{15}$$

and in which the dielectric constant, ε, is defined below

$$\sqrt{\varepsilon} = n \tag{16}$$

Equations (15) and (16) yield a relationship between the wave vector, K and the angular frequency, ω:

$$K = \frac{\omega}{c} \cdot n \tag{17}$$

Substituting for K to the equation (14) yields:

$$E_x = E_o \cdot e^{i(\omega t - \frac{\omega}{c} \cdot n \cdot z)} \tag{18}$$

Since the refractive index is complex for the absorbing medium, E_x has a form n + ik and

$$E_x = E_0 \cdot e^{i[\omega t - \frac{\omega}{c} \cdot (n + i \cdot k) \cdot z]} \tag{19}$$

One can then rearrange the terms of the equation (19) to obtain

$$E_x = E_0 \cdot e^{\frac{-\omega}{c} \cdot kz} \cdot e^{i \cdot \omega (t - \frac{n}{c} \cdot z)} \tag{20}$$

In the equation (20), the term $e^{\frac{-\omega}{c} \cdot k \cdot z}$ represents the absorbance. Hence the imaginary part of the index of refraction causes an exponential attenuation of the wave amplitude E_X.

2.4 Application of Fresnel reflection equations to SPR

The excitation of SPR is observed as a decrease in the reflection coefficient of the TM polarized light internally reflected off the sensing interface. A mathematical model using the plane-wave Fresnel reflection equations for an interface structure containing multiple planar layers can model the surface plasmon resonance condition. According to Fresnel's law, the reflected radiant power is influenced by the complex refractive index of matter, the angle of incidence, and the azimuthal angle of polarization. The ratio of refractive indices at the interface between two media governs the amount of radiation penetrating the interface. Thus, this reflected radiation contains information about the medium's absorption spectrum.

Fresnel's equations describe the reflection and transmission of electromagnetic waves at an interface. In the case of the SPR sensor, the reflection of the electromagnetic waves is considered. Light reflected from surfaces is characterized by two reflection amplitudes: r_p and r_s. The reflection amplitude r_p is for light polarization in the p direction (E in the plane of incidence). The reflection amplitude r_s is for light polarization in the s direction (E perpendicular to the plane of incidence and parallel to the surface) (Figure 1).

For a simple SPR sensor system with three layers of prism, metal and sensing material in the Kretschmann configuration, the Fresnel equation relating to p-polarization is:

$$r_{123,p} = \frac{r_{12,p} + r_{23,p} \cdot e^{2i \cdot K_{3z} \cdot d}}{1 + r_{12,p} \cdot r_{23,p} \cdot e^{2i \cdot K_{3z} \cdot d}} \quad (21)$$

$$r_{23,p} = \frac{K_{2z} \cdot \varepsilon_3 - K_{3z} \cdot \varepsilon_2}{K_{2z} \cdot \varepsilon_3 + K_{3z} \cdot \varepsilon_2} \quad (22)$$

and $$K_{jz} = \sqrt{\varepsilon_j \cdot \frac{\omega^2}{c^2} - K_x^2} \qquad \text{for j=1,2,3...} \quad (23)$$

ε_j and K_{jz} are the dielectric constant and the wave-vector component perpendicular to the interface in the j medium, respectively and d is the thickness of the metal layer. Layers 1, 2 and 3 are, respectively, the prism, the metal and the outer dielectric . The coefficients $r_{12,s}$ and $r_{12,p}$ give the strength of an electromagnetic wave reflected from an interface. The reflected light intensities (measured as light power) for p and s polarized light are given by:

$$R_P = \left| r_{12,p} \right|^2 \quad (24)$$

$$R_S = \left| r_{12,S} \right|^2 \quad (25)$$

Applying the Maxwell equations to the boundary conditions at the interface between the metal layer and the sensing layer, the surface plasmon wave propagates along the interface, with a wave-vector K_{SPR} given approximately as:

$$K_{SPR} = K_0 \cdot \sqrt{\frac{\varepsilon_S \cdot \varepsilon_m}{\varepsilon_S + \varepsilon_m}} \quad (26)$$

where ε_m and ε_s are the complex permitivities of the metal and sample, and the free space wave vector $K_0 = 2\pi/\lambda$. The complex permitivity is related to wavelength-dependent RI by:

$$\varepsilon = \varepsilon(\lambda) = \varepsilon'(\lambda) + i \cdot \varepsilon''(\lambda) = N(\lambda)^2 = (n(\lambda) + i \cdot k(\lambda))^2 \quad (27)$$

where n is the real RI and k is the imaginary RI component related to the optical absorption of the medium.

The light traveling through a medium with a RI of n_i at an angle to normal of θ_i has a wave vector of

$$K_x = K_0 \cdot n_i \cdot \sin(\theta_i) \quad (28)$$

The wave vector of the incident light will always have a value of $K_x < K_{SPR}$ as it has been explained in the dispersion curve. Therefore, a SPR wave cannot be excited by direct front-surface illumination of a smooth interface but rather by indirect (i.e. ATR) configurations.

If the energy and momentum conditions are right, the evanescent wave of the incident light generated at the prism-metal interfaces excites the surface plasmon at the outer metal-dielectric (i.e. sensing) interface. In a typical angle SPR scanning measurement, the reflectivity of a p-polarized light is measured as a function of incident angle. When the incident angle approaches the resonant angle, a pronounced minimum in the reflectivity curve occurs due to the energy transfer from the evanescent wave to the surface plasmon wave at the interface. SPR measurements yield film thickness and optical constants.

3. THEORECTICAL BASIS

3.1 Hypothesis

Conventional SPR measurements can be either reflectivity versus angle, $R(\theta)$, at a fixed wavelength or reflectivity versus wavelength, $R(\lambda)$, at a fixed angle. Both methods can determine, for example, the refractive index of a known adsorbed layer, or the thickness of an adsorbed layer of known refractive index, but not both. It is believed that analysis of the $R(\lambda,\theta)$ surface can yield spectral information characteristic of the near-surface analytes. The surface plasmon extinction band follows a curved trajectory on the $R(\lambda,\theta)$ surface as illustrated by the dark band in Figure 7 – experimental data for a gold film coated onto sapphire and contacting air. The apex of the extinction band corresponds to a maximum in the SPW coupling and therefore a maximal interaction between the incident light and the medium contacting the SPR sensor. We will show that in theory one can obtain the RI spectrum of the medium contacting the sensor, i.e. $(n(\lambda))$ and $(k(\lambda))$ by analyzing the $R(\lambda,\theta)$ surface, specifically modulation in the apex of the SPR extinction within the $R(\lambda,\theta)$ surface.

It is shown below that there is a phenomenological correlation between oscillations in the SPR angle $(\Delta\theta_{SPR}(\lambda))$ and oscillations in $n(\lambda)$ and, similarly, that oscillations in the reflectivity, measured at the apex of the SPR curve $(\Delta R_{SPR}(\lambda))$ closely resemble $k(\lambda)$. Hence, the reflectivity surface can reveal the optical constants and thus provide a spectral fingerprint of analytes contacting

the SPR sensor surface. This qualitative fingerprint information supplements the quantitative angle or wavelength shift information of a conventional SPR sensor and provides an important internal spectral validation of the experiment. Such a spectral fingerprint might be used to identify or discriminate between different analytes.

3.2 Summary of the theoretical approach

The computation of the oscillations in $\Delta\theta_{SPR}(\lambda)$ and $\Delta R_{SPR}(\lambda)$ for the model analyte isoamyl alcohol were the main results of this study. First, the $k(\lambda)$ data were obtained from a literature spectrum and then converted to $n(\lambda)$ data via KKT. Second, a function to return the complex refractive index, $N(\lambda)$, for isoamyl alcohol was constructed. Third, the complex RI of isoamyl alcohol was used in Fresnel simulations to compute the theoretical reflectivity surface $R(\lambda,\theta)$ for the following stratified interface: sapphire (n=1.75) | Au(50 nm) | fictitious solvent (n=1.40), or isoamyl alcohol. Fourth, the set of SPR angles, $\theta_{SPR}(\lambda)$ were calculated from this surface for a finely spaced set of wavelengths. Fifth, a set of data corresponding to $\Delta\theta_{SPR}(\lambda)$ and $\Delta R_{SPR}(\lambda)$ for the exchange of the non-dispersive, fictitious solvent with isoamyl alcohol was constructed. Finally, $\Delta\theta_{SPR}(\lambda)$ and $\Delta R_{SPR}(\lambda)$ were compared to the $n(\lambda)$ and $k(\lambda)$ spectra of isoamyl alcohol for the purpose of obtaining a phenomenological correlation between the measurement and the analyte spectral properties.

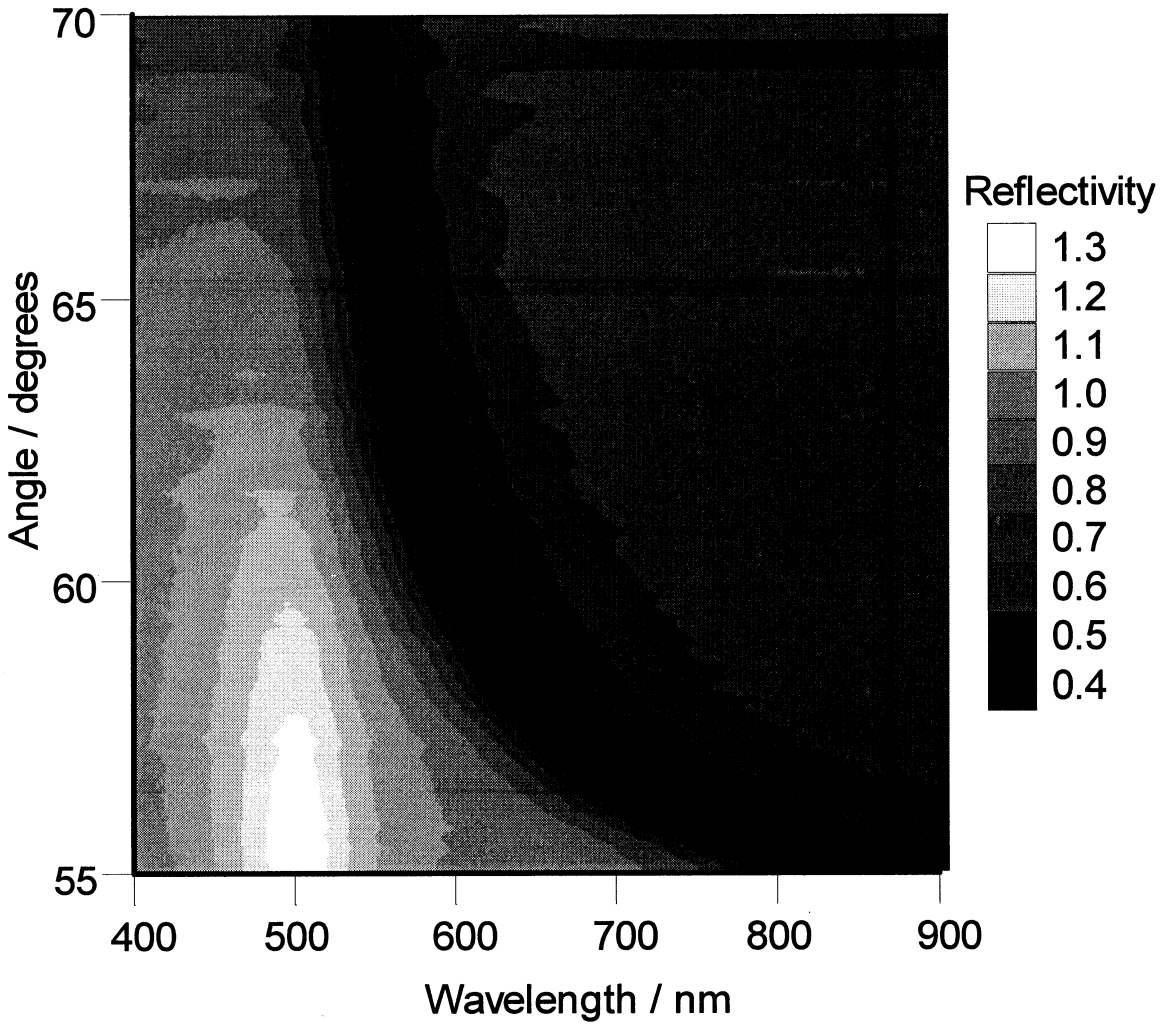

Figure 7: Reflectivity surface. Reflectivity is plotted in grayscale (white = high reflectivity, dark = low reflectivity) as a function of angle and wavelength illustrating the curved trajectory of the surface plasmon absorption band (black curve) when viewed in this space.

3.3 Fresnel calculations

Fresnel reflectivity calculations of a 4-layer system was derived by Bohn [15] and translated into a Mathcad 2001® worksheet by Terrill [16]. The first layer is sapphire, the second one is gold, the third one an analyte and the fourth one a solution. In the SPR-coupled-ATR experiment, Fresnel simulations were based on sapphire | Au (50nm) | ISA for the absorbing analyte case and sapphire | Au (50nm) | acetone using a fictitious, nondispersive RI for the reference spectrum. The analyte layer was intentionally set to zero thickness so that it had no effect on the reflection calculation – reducing these to 3-layer calculations. The goal was to simulate the response to the bulk solution layer. For comparison, the same configuration minus the Au gold layer was simulated – equivalent to a simple attenuated total reflection experiment that does not benefit from SP resonance. The wavelength dependent optical constants ($n(\lambda)$ and $k(\lambda)$) were derived from a polynomial interpolation model, written in Mathcad by Terrill, by taking data from various sources [17].

3.4 Data analysis

3.4.1 Absorbance spectrum, k(λ)

A near infared spectrum of ISA was obtained from Anderson Near Infared Spectra of the Anderson Physical Laboratory in Champaign, Illinois. Absorbance was converted to the imaginary refractive index, k by the formula

$$k = 2.303 \cdot A \cdot \frac{\lambda}{4 \cdot \pi \cdot b} \tag{29}$$

where A is the absorbance and b is the path length. k values were interpolated so that they fell on even numbered intervals on the wavenumber axis. This step ensured that the k-data had 2^n values, a requirement for fast Fourier transform (FFT) routines.

In some cases it was necessary to apodize the absorbance data such that it fell smoothly to zero before and after the peak(s) in the data. Apodization must be experimentally determined because too broad of a roll-off will distort the data and too sharp of a roll-off will create spurious peaks.

3.4.2 Kramers-Kronig transform of n(λ)

The n(λ) spectrum was derived from the k(λ) via a process equivalent to the Kramers-Kronig transform (KKT) as described by Bertie et al [8]. The complex refractive index N(λ) of isoamyl alcohol was then used in the Fresnel equations to compute the R(λ,θ) surface.

4. RESULTS AND DISCUSSION

In a conventional ATR reflectivity experiment, once the angle of incidence is greater than the critical angle, reflectivity reaches unity (Figure 8A). But in the SPR-coupled ATR reflectivity experiment, a sharp loss of reflectivity is observed when the light energy interacts with the SPW along the metal-dielectric interface under resonant conditions (Figure 8B). Monitoring shifts in the resonant angle as

a function of wavelength can characterize the complex refractive index of the material in contact with the metal surface. Figure 9 illustrates the wavelength dependence of the angle corresponding to the apex of the SPR minimum in the near infrared simulated for a 50 nm Au film on sapphire and contacting isoamyl alcohol. Qualitatively this curve resembles those derived from visible wavelength calculations, but the overall change in angle is smaller - 56.65^0 to 55.3^0 for wavelengths from 1100 nm to 2100 nm. The overwhelming contributors to the overall shape of this curve are the optical constants of gold and sapphire.

The simulations in this study suggest two kinds of analyses of the SPR reflectivity surface: measurements of oscillations in the wavelength dependent resonance angle - $\Delta\theta_{SPR}(\lambda)$ - and oscillations in the depth of the reflectivity apex - $\Delta R_{SPR}(\lambda)$, both measured relative to a reference state (i.e. a blank). The reference state in our simulations is a fictitious solution layer with a featureless real refractive index of n = 1.40. The model analyte layer is isoamyl alcohol. The complex refractive index of isoamyl alcohol is derived from a reference spectrum. The imaginary part, $k(\lambda)$, is a simple algebraic derivative of the absorbance function $A(\lambda)$:

$$k(\lambda) = 2.303 \cdot A(\lambda) \cdot \frac{\lambda}{4 \cdot \pi \cdot b} \qquad (30)$$

The real part, $n(\lambda)$ is computed in turn via the KKT of $k(\lambda)$. Together $n(\lambda)$ and $k(\lambda)$ are plotted in Figure 10. The $k(\lambda)$ and $n(\lambda)$ spectra are qualitatively correct – $k(\lambda)$ directly mirrors the absorption bands and $n(\lambda)$ exhibits the

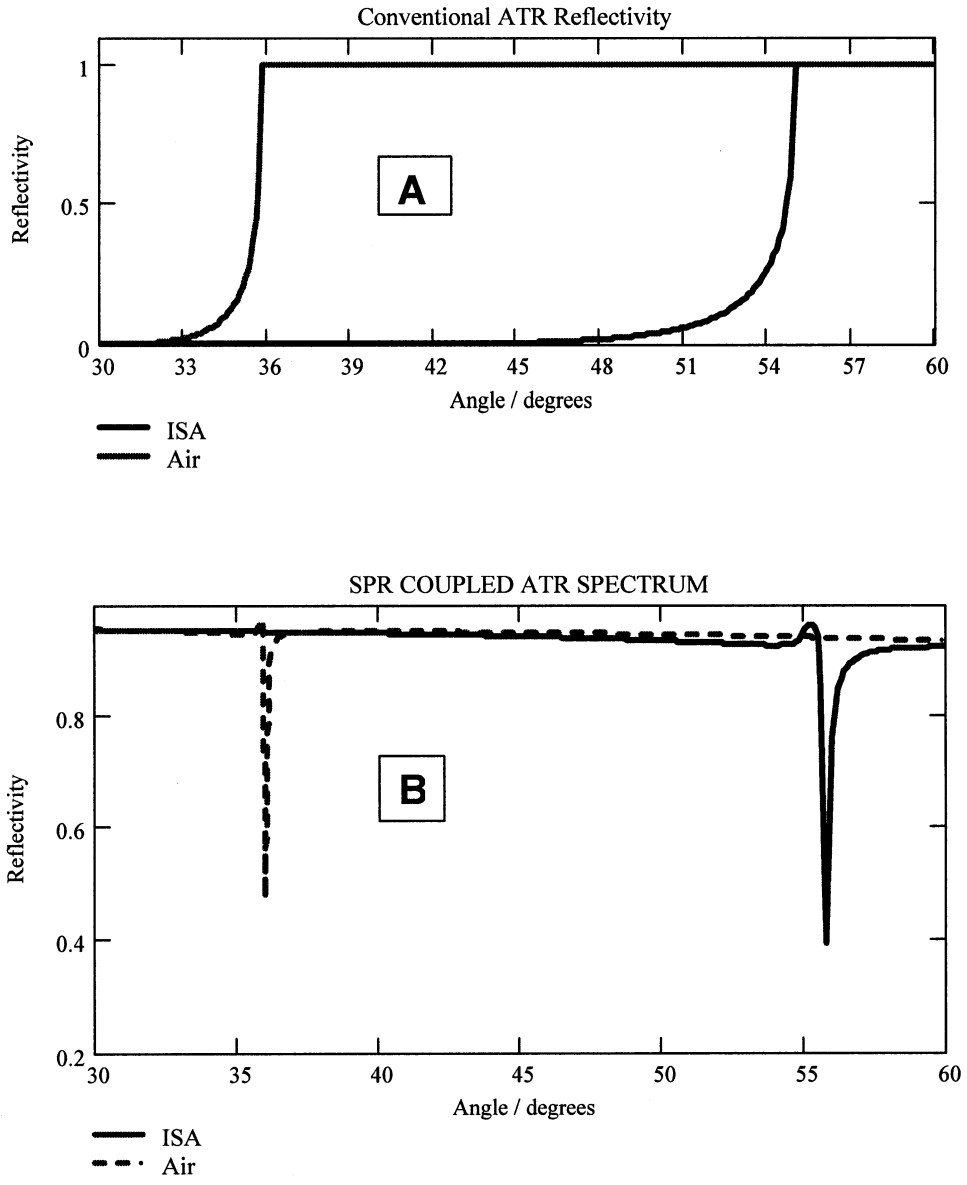

Figure 8: Attenuated total reflectivity (ATR). A. Conventional ATR. B. SPR-coupled ATR.

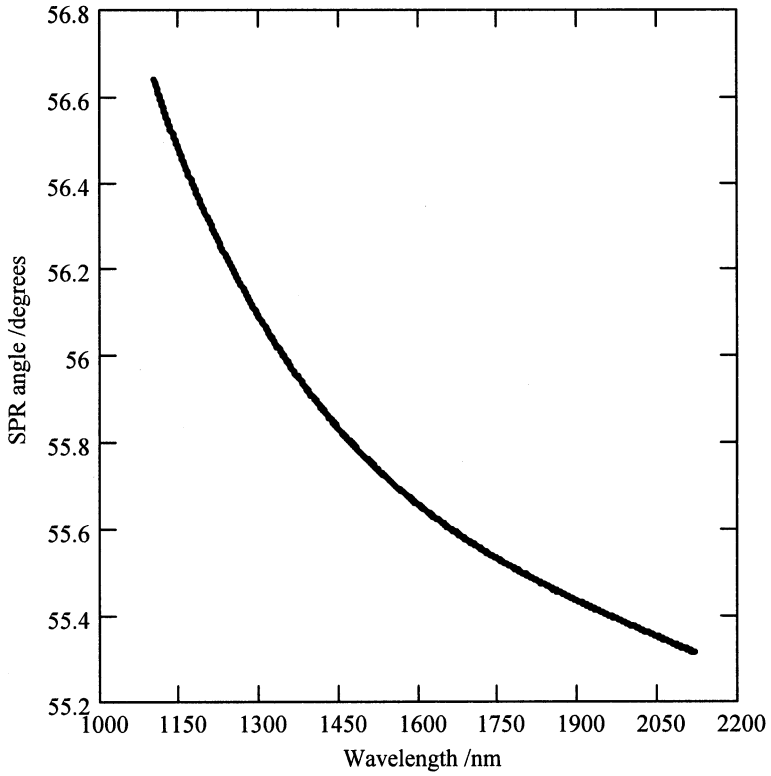

SPR angle as a function of wavelength

Figure 9: Wavelength dependence of angle corresponding to the apex of the SPR minimum in the near infrared. Simulation conditions are sapphire | Au | isoamyl alcohol.

expected quasi-derivative form. The desired reflectivity changes, $\Delta\theta_{SPR}(\lambda)$ and $\Delta R_{SPR}(\lambda)$ are computed using the isoamyl alcohol $N(\lambda) = n(\lambda) + ik(\lambda)$ data and subtracting the corresponding calculations that use the fictitious (n=1.40) blank for the solution layer. The $\Delta\theta_{SPR}(\lambda)$ data are plotted in Figure 11. Significantly, $\Delta\theta_{SPR}(\lambda)$ is nearly identical in form to $n(\lambda)$ – so experiments that measure $\Delta\theta_{SPR}(\lambda)$ will serve to directly measure $n(\lambda)$ given the proper scaling information. For isoamyl alcohol however the peak oscillations were small – approximately 10^{-4} degrees and this may be hard to measure. The problem originates in the small oscillations in $n(\lambda)$ – ca. $2x10^{-6}$ refractive index units – that are typical of the vibrational overtones that populate the NIR frequency spectrum. These small oscillations are in turn a function of the weak NIR absorptions – the peak $\varepsilon(\lambda)$ magnitudes for isoamyl alcohol in this range are $3.7x10^{-6}$, $1.3x10^{-6}$, $9.3x10^{-7}$ and $1.5x10^{-6}$ $M^{-1}cm^{-1}$.

Figure 11 shows the similarity between the $n(\lambda)$ spectrum of the analyte and the $\Delta\theta_{SPR}(\lambda)$ spectrum. This type of result was recently reported by Tao et al. [13] for measurements in the visible range for cytochrome-C, a strong visible-λ chromophore that was adsorbed to Au. Tao et al. used a specialized instrument that makes such measurements in the mid visible wavelengths with high angle resolution. Their instrument was able to record $\Delta\theta_{SPR}(\lambda)$ spectra for an adsorbed phthalocyanine layer with a resolution near 10^{-4} degrees. The value of such a measurement is that it provides an *in-situ*, non-destructive spectral

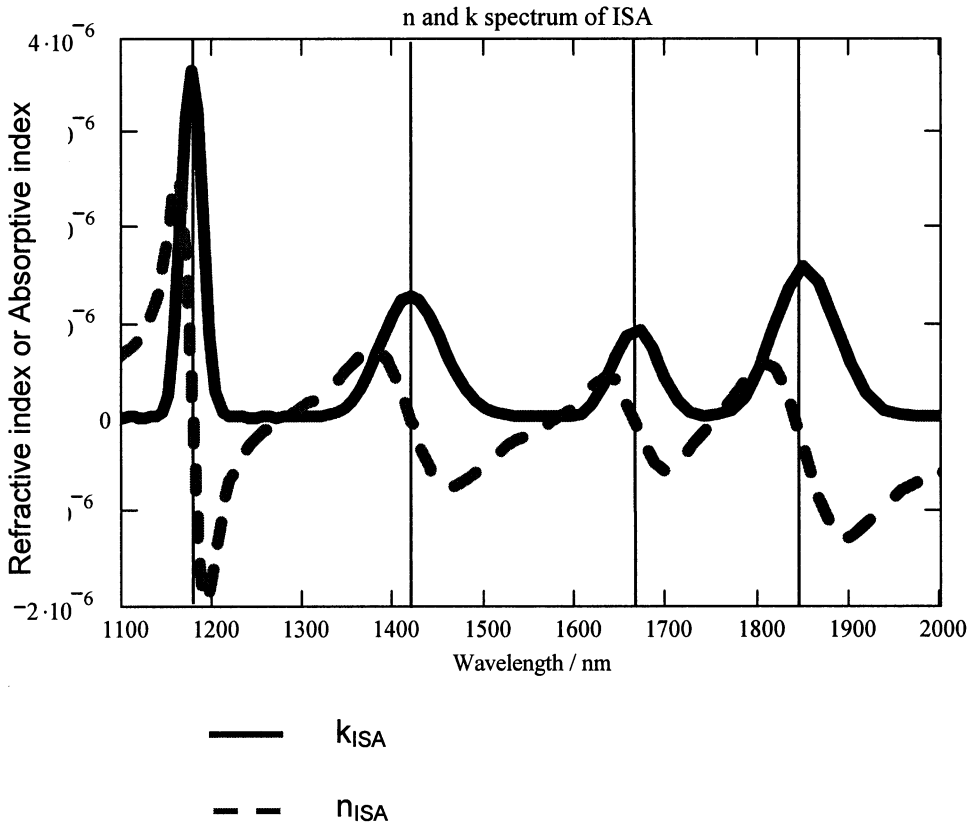

Figure 10: Refractive index spectrum, n(λ) and absorbance spectrum of isoamyl alcohol, k(λ). The n(λ) spectrum has kinks around the absorbance peaks (λ_{max} = 1178, 1418, 1670 and 1849 nm).

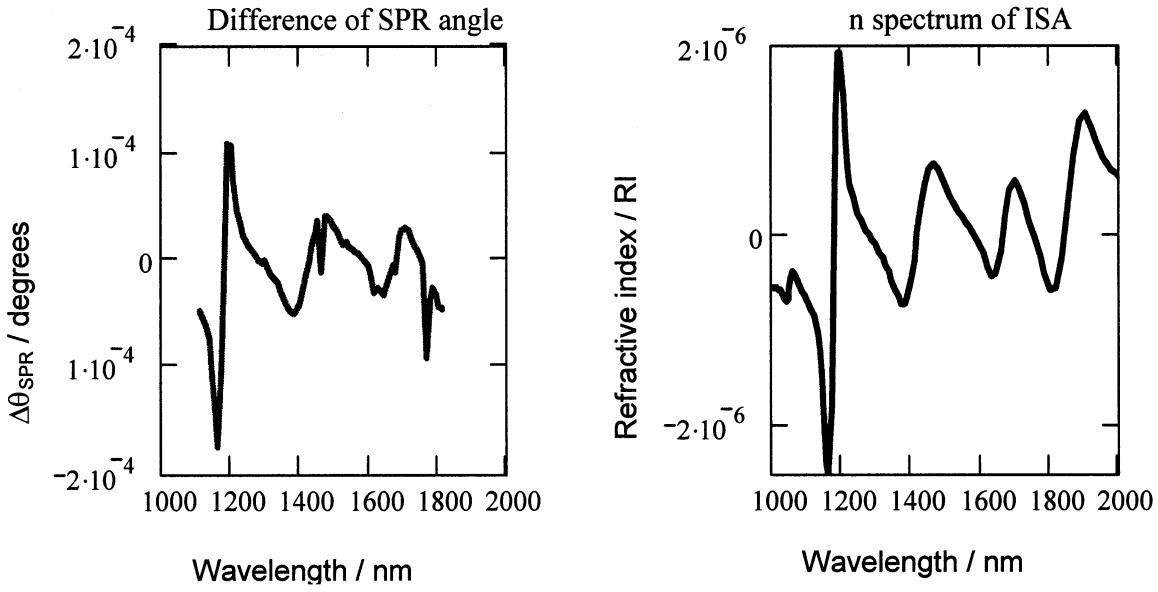

Figure 11: Plot comparisons of $\Delta\theta_{SPR}(\lambda)$ and $n_{ISA}(\lambda)$.

validation to accompany the typically 1D SPR signal. Visible wavelength chromophores are fairly rare however, hence the need to characterize analytes in a spectral region where nearly *all* molecules have unique absorption spectra.

The complement to the $n(\lambda)$ spectrum is the $k(\lambda)$ spectrum. Since $k(\lambda)$ is related to light absorption, its phenomenological counterpart appears not in $\theta_{SPR}(\lambda)$ but rather in the reflectivity itself, $R_{SPR}(\lambda)$. The change in $R(\lambda)$, at a fixed angle of 55 degrees, and between a fictitious blank and isoamyl alcohol are illustrated in Figure 12.

Figures 13, 14 and 15 illustrate a set of curves of $R(\lambda)$ at a fixed incident angle that is slightly below, on and above the angle for which SP resonance occurs – i.e. a series of slices (horizontal on Figure 7) through the $R(\lambda,\theta)$ surface as it traverses the SP resonance.

Slightly off-resonance at $\theta > \theta_{SPR}$ the $\Delta R(\lambda)$ spectrum clearly resembles $k(\lambda)$ spectrum as would be expected for this type of attenuated total reflection experiment – see Figure 13. The very small magnitudes are attributable to the Au layer that reduces the interaction between the light and the solution. Figure 14 explores the angles where the SP resonance passes through the illustrated spectral range. As the incident angle is decreased to 56.45°, the SP resonance appears at 1000 nm and quickly shifts to 2000 nm during the next -1° angle shift. The effect of the SPR coupling is two-fold. Firstly, it magnifies the coupling to the solution layer by a factor of approximately 100 and secondly, it has the effect of dramatically modulating the band-shapes. The peaks in changing from negative

ΔR, to bipolar and to positive as the SP resonance traverses the peak from high θ (low λ) to low θ (high λ). Note that this effect is due to the perturbation of the absorption peaks alone. At angles greater than the resonant angle, the $\Delta R(\lambda)$ spectrum again resembles the $k(\lambda)$ spectrum but the magnitude of the ΔR oscillations decreases even further (Figure 15).

Figure 16 is a comparison of the above described SPR-coupled ATR experiment and one that might be done with in a conventional way, i.e., without the Au film. To make this comparison, we fixed the simulation angle at 55.7°, which placed the SP resonance squarely in the middle of the spectrum at 1500 nm. This angle was then used to simulate $\Delta R_{SPR}(\lambda)$ as above as well as $\Delta R(\lambda)$ computed in the same way but *without* the Au layer. The latter simulation corresponds to a conventional ATR absorption spectrum. The k spectrum of ISA is plotted alongside for reference (dashed line). The primary observation is that the $\Delta R_{SPR}(\lambda)$ data are quite comparable to the conventional $\Delta R(\lambda)$ ones but exhibiting distorted band shapes near 1500nm along with a ca. 4-fold increase in magnitude. The peak magnitudes are modestly diminished off-resonance but nearly normal in shape.

5. CONCLUSION

These simulations indicate that if a near-surface analyte has a characteristic absorbance peak, it will be possible to use SPR-coupled ATR to simultaneously measure both its refractive index $n(\lambda)$ and absorbance $k(\lambda)$

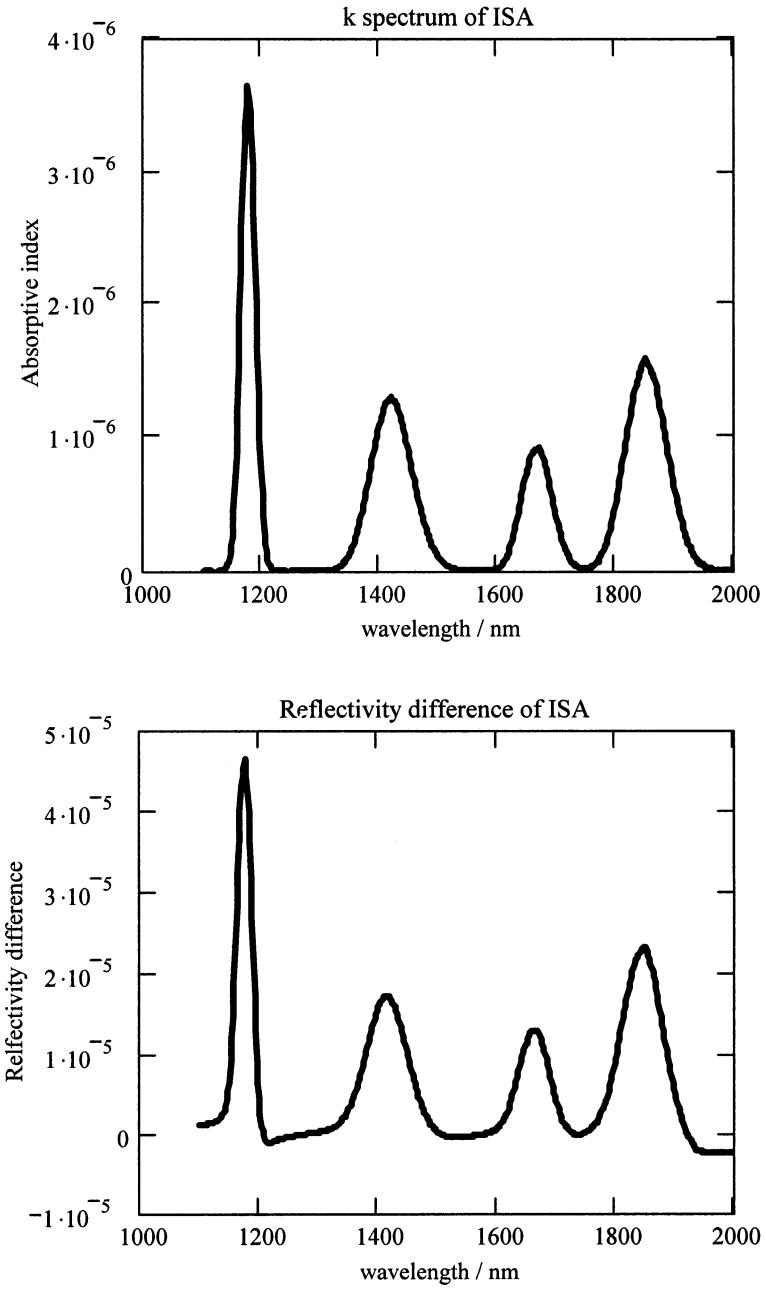

Figure 12: Plot comparisons of $\Delta R(\lambda)$ and $k_{ISA}(\lambda)$. The $\Delta R(\lambda)$ is at angle of 55 degrees.

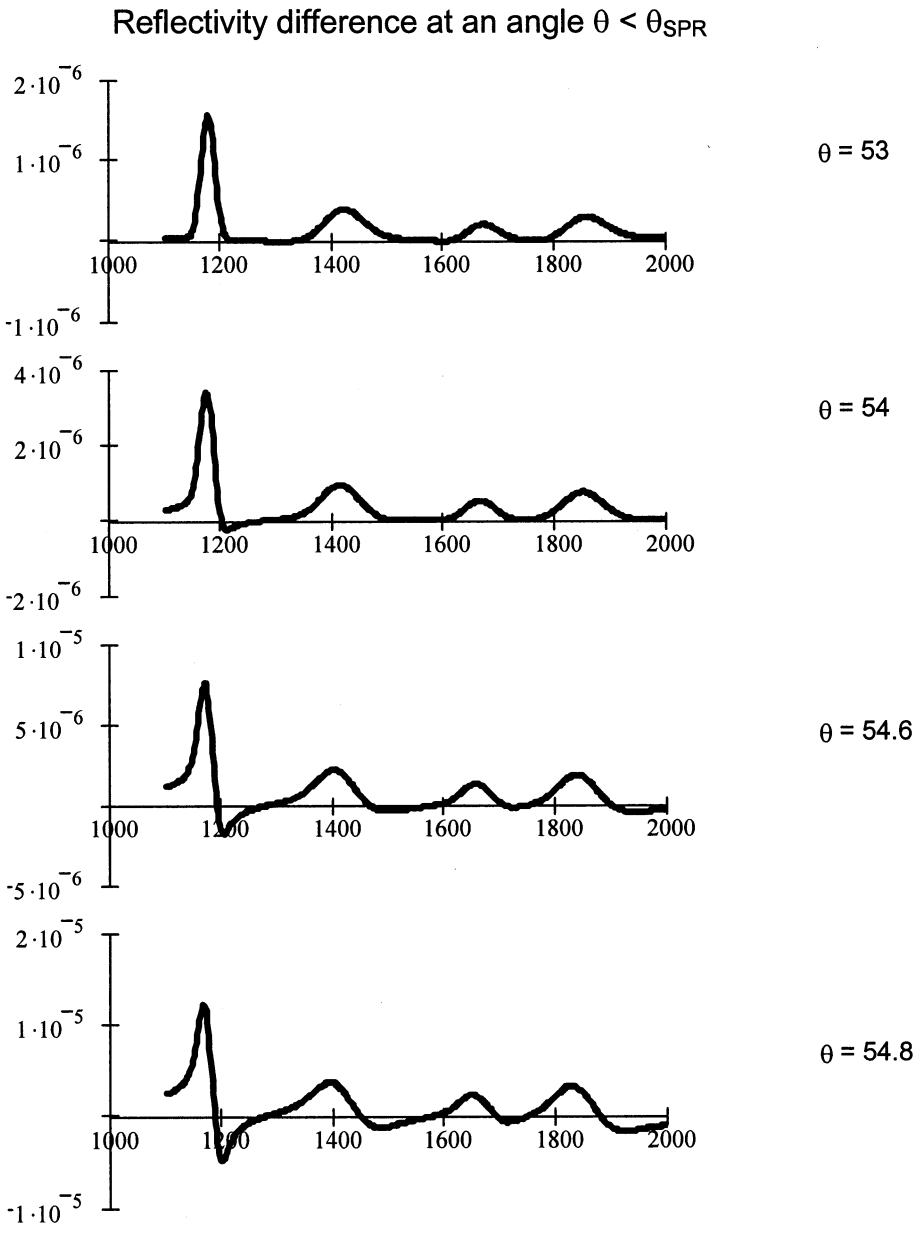

Figure 13: A set of curves of ΔR(λ) at fixed angles of 53^0, 54^0, 54.6^0, and 54.8^0. These angles are below the SPR angle.

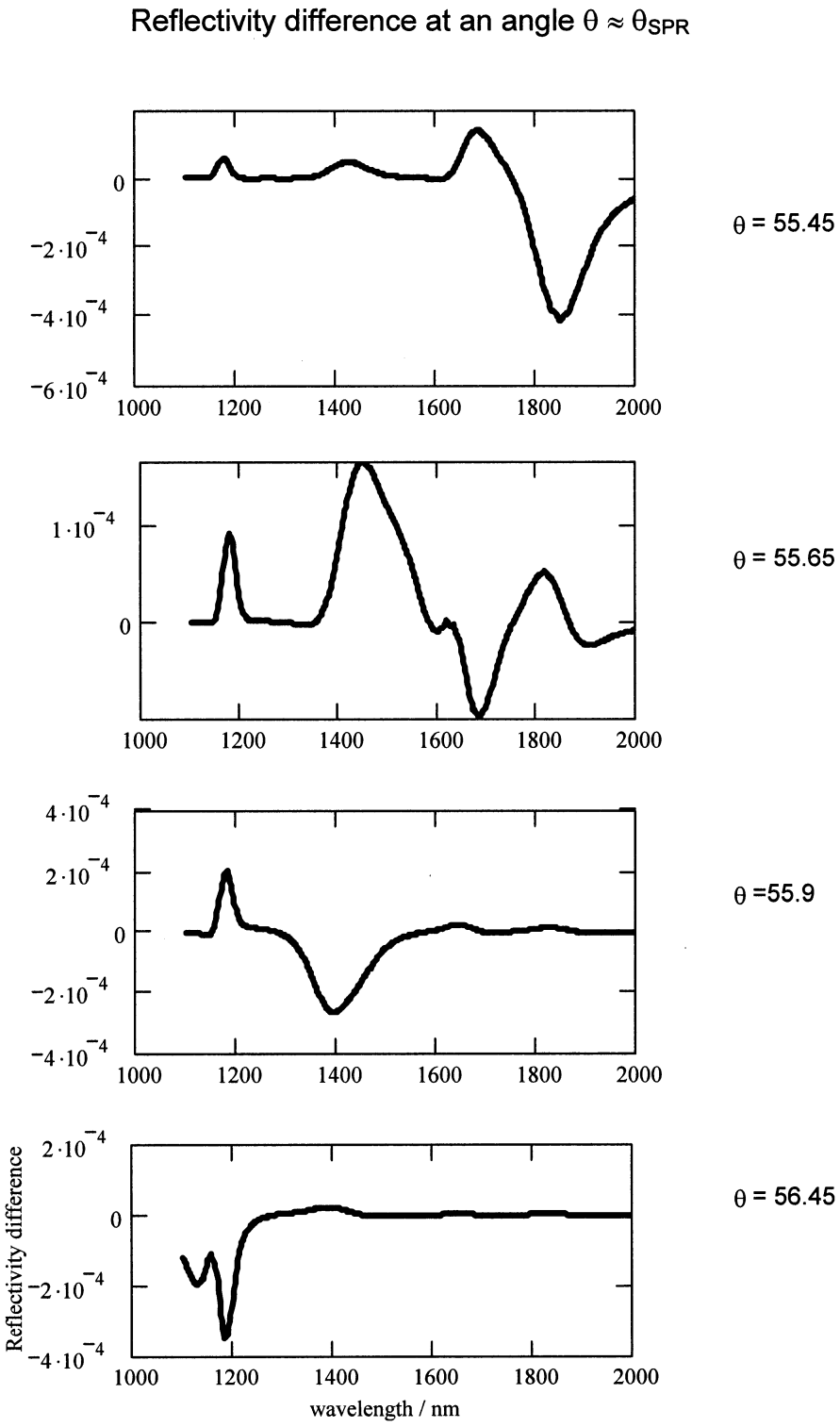

Figure 14: A set of curves of $\Delta R(\lambda)$ at fixed angles of 55.45^0, 55.65^0, 55.9^0, and 56.45^0. These angles are on the SPR angle.

Reflectivity difference at an angle $\theta > \theta_{SPR}$

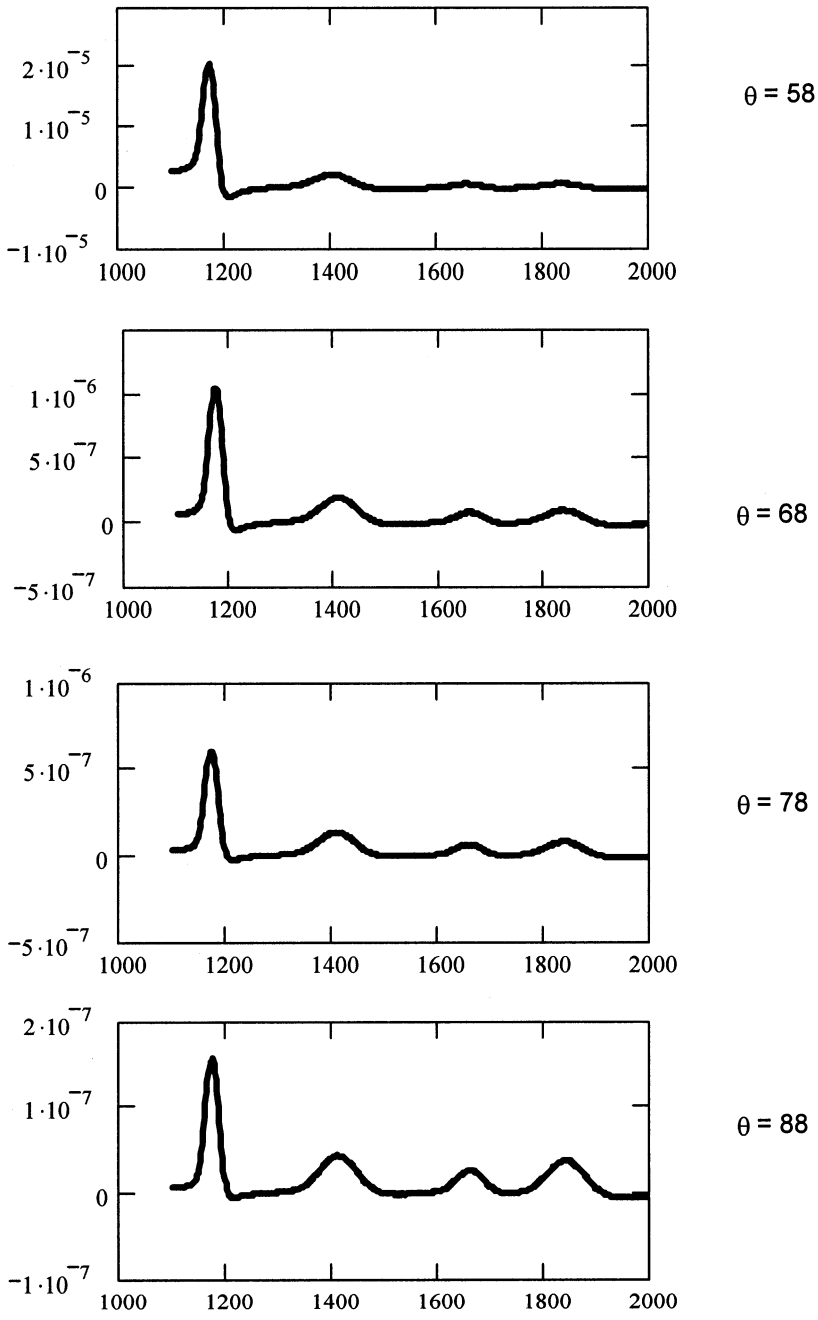

Figure 15: A set of curves of $\Delta R(\lambda)$ at fixed angles of 58^0, 68^0, 78^0, and 88^0. These angles are above the SPR angle.

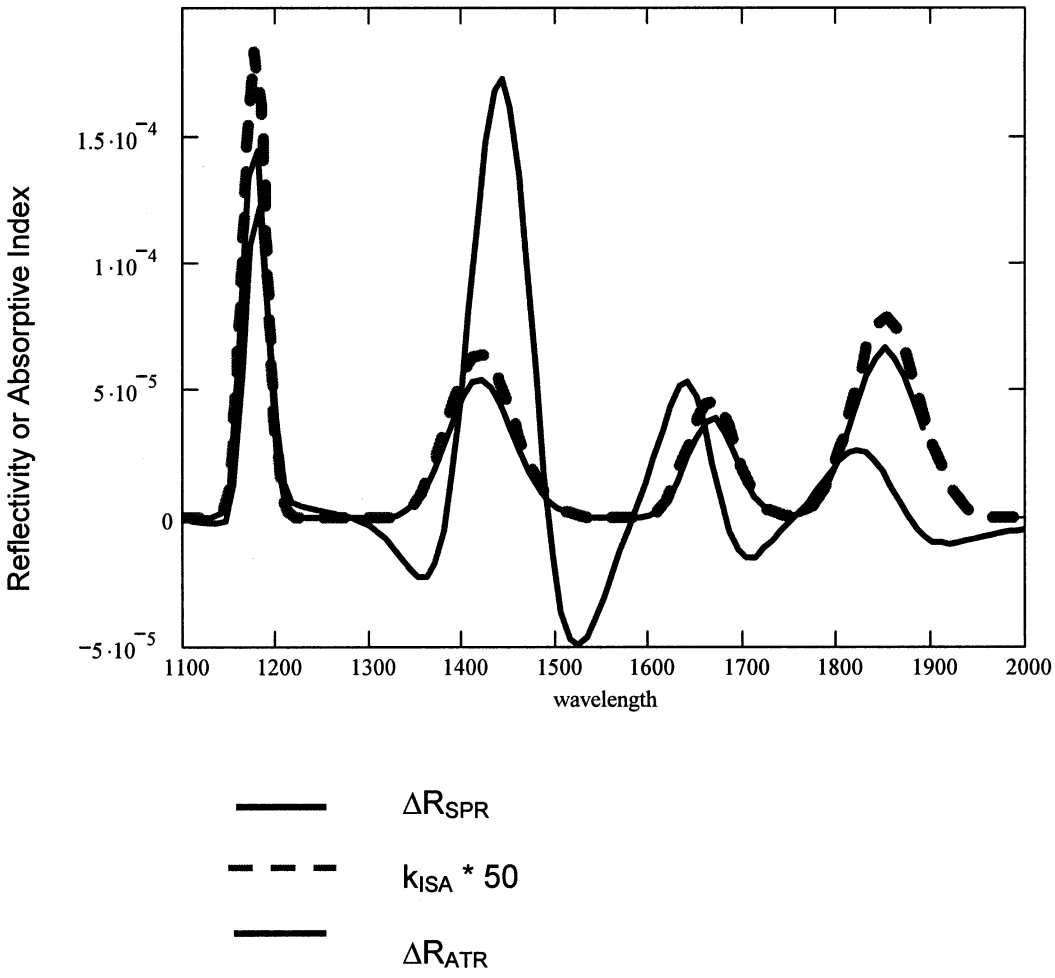

Figure 16: Comparison of ΔR spectra of 2 types of theoretical experiments and k_{ISA}, absorptive spectrum. The magnitude of k_{ISA} spectrum is magnified 50 times. The angle $\theta_{SPR} = 55.7^0$ at $\lambda = 1500nm$ was used to construct the reflectivity spectra in the analysis of ΔR_{SPR}.

spectra by analysis of the SPR coupled reflectivity surface. The SPR-coupled ATR method being more sensitive than a conventional one, but at the cost of experimental complexity. The SPR coupled method will be responsive to both the real and imaginary parts of the dielectric function of the analyte and as such may provide a method for leveraging selectivity into more conventional SPR experiments. However, the very weak absorbance bands present in the NIR make these oscillations small compared to the anticipated minimum detectable ΔR and $\Delta\theta$ of the SPR reflectometer, so an alternative methodology should be pursued.

A promising direction to pursue is to do the same simulations / experiments in the infrared frequency region where the operative extinction coefficients are many orders of magnitude larger. The practical consequences of this are increased solution background absorption, instrument cost and more stringent optical (i.e., numerical aperture) and angle control requirements since the width of the SP resonance in the mid-IR is only a small fraction of a degree.

REFERENCES

1. Georgiadis, R.; Peterlinz, K. A. *Langmuir* **1996**, *12*, 4731-4740.

2. Georgiadis, R.; Peterlinz, K. A. *J. Phys. Chem. B* **1997**, *101*, 8041-8042.

3. Chinowsky, T. M.; Yee, S. S.; *Sensor and Actuators B* **1998**, *51*, 321-330.

4. Kang, X.; Jin, Y.; Cheng, G.; Dong, S. *Langmuir* **2002**, *18*, 1713-1718.

5. Nedelkov, D.; Nelson, R. W.; Tubbs, K. A. *Anal. Chem.* **2000**, 404A-411A.

6. Beloglazov, A. A.; Creighton, J. A.; Nikitin, P. I.; Smith, A. M.; Sommerdijk, N. A. J. M.; Valeiko, M. V.; Wright, J. D. *Sensors and Actuators B* **1997**, *38-39*, 53-57.

7. Bornmann, A.; Westphal, P. *Sensors and Actuators B* **2002**, *84*, 278-282.

8. Kramers-Kronig Transformation is implemented via serial Fourier transforms as outlined in **a**. Bertie, J. E.; Eysel, H. H. *Appl. Spectrosc.* **1985**, *39*, 392 **b**. Ahmed, M. K.; Bertie, J. E.; Eysel, H. H.; Harke, H. *Croatica. Chem. Acta* **1988**, *61*, 391 **c**. Bertie, J. E.; Manji, R.; Zhang, S. L. *Appl. Spectrosc.* **1992**, *46*, 1660.

9 . Knoll, W. *Annu. Rev. Phys. Chem.* **1998**, *49*, 569-638.

10. Kretschmann, E.; Raether, H. *Z. Naturforsch* **1968**, *23A*, 2135-3136.

11. Otto, A. *Z. Physik* **1968**, *216*, 398-410.

12. Bertie, J.E. Optical constants from the handbook of vibrational spectroscopy, **2001** John Wiley & Sons.

13. Boussaad, S.; Pean, J.; Tao, N. J. *Anal. Chem.* **2000**, 72, 222-226.

14. Gasiorowicz, S.; Fishbane, P. M.; Thornton, S. T. Physics for Scientists and Engineers, **1993** Prentice hall.

15. Bohn, P.W. "Laser Applications in Chemistry and Biophysics" Proceedings of the SPIE-International Society for Optical Engineering, 1986.

16. Terrill, R. H. wrote the SPR Fresnel's calculations in Mathcad, based on the derivation of the 4-layer system by Bohn. A copy of the Mathcad worksheet can be obtained from Terrill.

17. Wavelength dependent optical constants were modeled by polynomial interpolation of data taken from the following sources: Gold. The Robert M. Corn research group at (http:// corninfo.chem..wisc.edu/). Sapphire. Oriel instruments Inc. 2001 product catalog. Oriel instruments, 150 Long Beach Blvd. Stratford, CT 06615-0872 (www.oriel.com). Chromium and water. The CRC Handbook of Chemistry and Physics, 76th Edition © 1995, CRC Press.

APPENDIX A
KRAMERS-KRONIG TRANSFORMATION OF ISOAMYL ALCOHOL (ISA)

This worksheet implements the Kramers-Kronig transform (KKT) which transforms suitable absorbance into refractive index index spectra. This is the first step in the experimental approach.

The absorbance data used below were reconstructed from the NIR spectrum of isoamyl alcohol from the Anderson Physics Laboratory

1. This is the working template of dfft with 2^9 = 512 data points when the data points of the original data is greater than 256 points and
less than 512 points.

w (cm-1) = wavenumber = 10^4/ λ (μm)

A = absorbance = log (100/ %T)

This formula was used to convert the A (absorbance) data to k:

$$k = 2.303 \cdot A \cdot \frac{\lambda}{(4 \cdot \pi \cdot b)}$$

wnk is an imported excel file. It contains the wavelength and k data of isoamyl alcohol.

wnk :=

F:\..\112pt_nubarkisoamylalcohol021003.xls

rows(wnk) = 112 pt := rows(wnk) x := 0.. (pt − 1)

$k\_original_x := wnk_{x,1}$ $w\_original_x := wnk_{x,0}$ $n\_original_x := wnk_{x,1}$

The functions below are used to interpolate the k-data so that they fall on even wavenumber intervals in w1. It is very important that kinterp have 2^n values for the fft routines below.

Range for the frequency values

jj := 0.. pt − 1 jjmax := pt − 1 $w\_original_0 = 4.587 \times 10^3$

$\text{rows}(k\_original) = 112$ $\qquad w\_original_{jjmax} = 1 \times 10^4$

$$dw := \frac{w\_original_{jjmax} - w\_original_0}{pt} \qquad dw = 48.329$$

Evenly spaced wavenumber array

$$w1_x := w\_original_0 + dw \cdot x$$

g(wavelength range, peak width,wavelength peak), a gaussian equation, is used to produce smooth (Gaussian) peaks as illustrated by the dotted lines in the figure

$$g(v,\sigma,\mu) := 500 \cdot \sqrt{\frac{1}{2 \cdot \pi \cdot \sigma^2}} \cdot e^{-\frac{(v-\mu)^2}{(2 \cdot \sigma)^2}}$$

$$k\_syn := g(w1,70,5400) \cdot 145 + g(w1,45,8520) \cdot 380 + g(w1,70,6000) \cdot 100 \ldots$$
$$+ g(w1,200,8400) \cdot 150 \ldots$$
$$+ g(w1,140,7000) \cdot 300 + g(w1,50,9450) \cdot 50$$

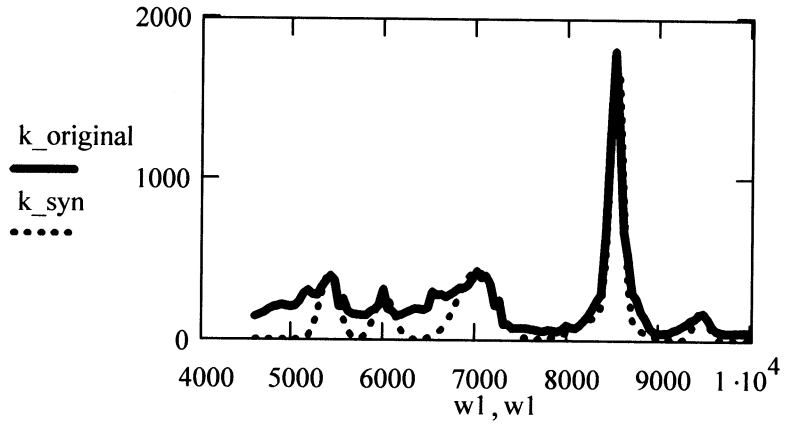

In cases where the absorbance data do not span an absorbance peak cleanly and return to near zero absorbance on both sides, it is best to apodize the absorbance data such that it smoothly falls to zero before and after the peak(s) in the data. This roll-off must be experimentally determined because too sharp a roll-off will create spurious peaks in the KKT, but too broad of a roll-off will distort the data somewhat.

Apodization function for absorbance data so FFT does not 'ring'.

$AS := 45$ start apodization

$std := 6$ std deviation of gaussian for smooth

$$rhs_{jj} := \left(pnorm\left(jj, \frac{AS}{4}, std \right) \cdot if(jj < AS, 1, 0) + 1 \cdot if(jj \geq AS, 1, 0) \right)$$

$$AP_{jj} := if\left[jj \geq (jjmax - AS), pnorm\left[-jj, -1 \cdot \left(jjmax - \frac{AS}{4} \right), std \right], 1 \right] \cdot rhs_{jj}$$

$k\_syn_x := k\_syn_x \cdot AP_x$ $maxk := max(k\_original)$

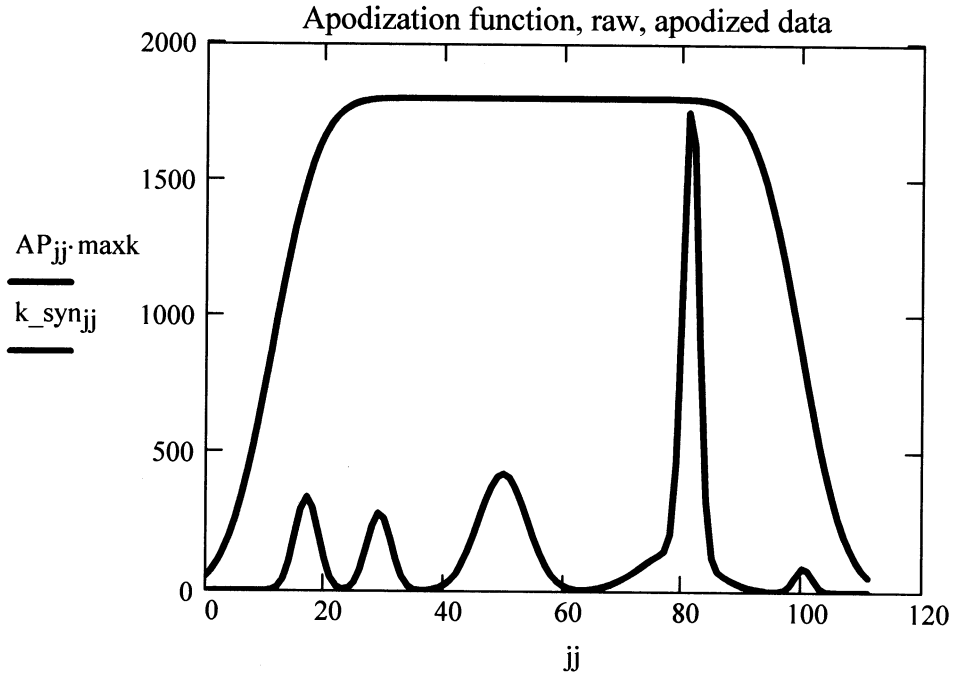

In the next section, the data are prepared for KK Transformation. This requires that they be reflected along both the wavenumber and k axes, and then extended to 2n points.

Smoothing distorts the data set and should only be used when random noise would otherwise make the fits worse.

$k\_synR_x := (-k\_syn)_{(pt-1)-x}$

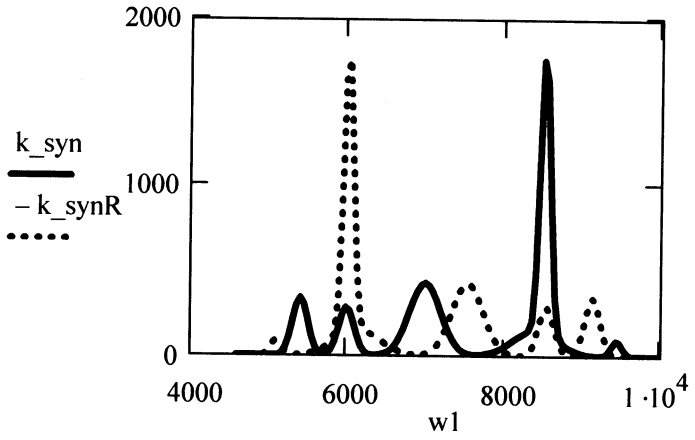

rows(w1) = 112

qq := rows(w1) qq = 112

kr := stack(k_syn, k_synR) q := 0.. (qq·2) – 1

$wt_q := (q - qq)$ rows(k_synR) = 112 rows(wt) = 224

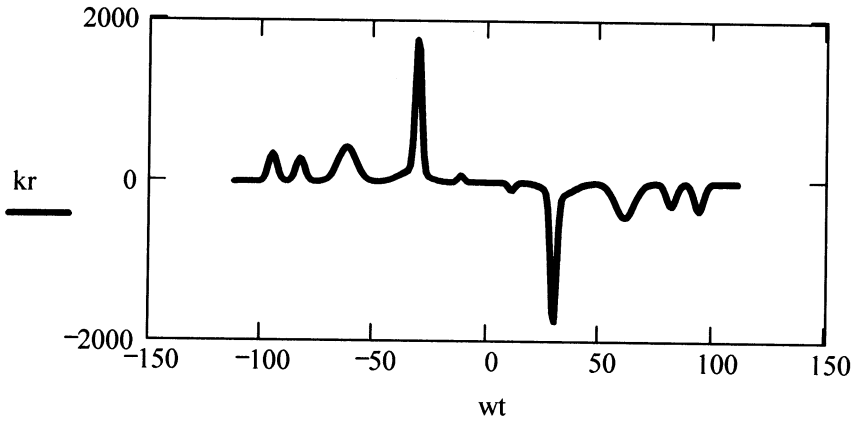

$i := 0..15$ $zz := 0..255$

$zero_i := 0$ $wtR_x := wt_x$ $k\_synR_x := (-k\_syn)_{(pt-1)-x}$

$wzeroleft_i := -128 + i$ $rows(wzeroleft) = 16$

$wzeroright_i := (112 + i)$ $rows(wzeroright) = 16$

$ww2 := stack(wzeroright, wtR)$ adding zero points to one end of the file

$ww3 := stack(wzeroleft, ww2)$ adding zero points to the other end of the file

$k2 := stack(kr, zero)$ adding zero points to one end of the file

$k3 := stack(zero, k2)$ adding zero points to the other end of the file

The k data of isoamyl alcohol is transformed by double fast fourier transform. Double fast fourier transform is equivalent to Kramers-Kronig tranformation.

$cc := cfft(-fft(Re(k3)))$ Serial fast fourier transforms - second must be complex fft because the first fft creates complex number output

$u := 0..512$ $t_u := u$

$nd := Im(cc)$ Here is the refractive index

$kd := Re(cc)$ Here are the recreated k values

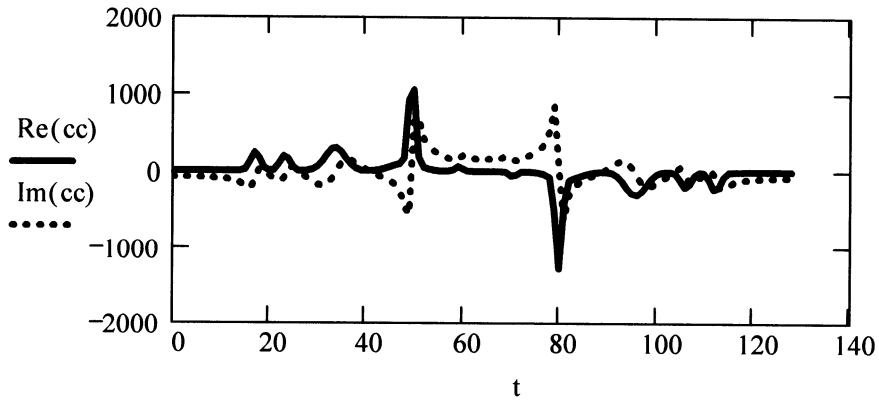

Now we must re-create a wavenumber axis for these data.

$\text{length}(nd) = 129$ $\quad ll := \text{length}(nd)$

$nd := \text{submatrix}\left(nd, 0, \frac{ll}{2}, 0, 0\right)$ take the first half of the data

$kd := \text{submatrix}\left(kd, 0, \frac{ll}{2}, 0, 0\right)$ $\quad zz := 0 .. \frac{ll}{2}$ make a range variable

Now recreate the actual wavenumbers for the nd data set - the reason that this must be done is that there are half as many point in nd as there are in kinterp.

$$wd_{zz} := w1_0 + 2\frac{\left(w1_{\text{length}(w1)-1} - w1_0\right)}{\text{length}(w1)} \cdot (zz)$$

recover 256 points by interpolation

$SS := \text{cspline}(wd, nd)$ $\quad TT := \text{cspline}(wd, kd)$

$ndi := \text{interp}(SS, wd, nd, w1)$ $\quad kdi := \text{interp}(TT, wd, kd, w1)$

$kdi := kdi$ $\quad n_\alpha := 1.45$ $\quad ndi := ndi + n_\alpha \cdot \frac{6.198}{4.373} = 1.417$

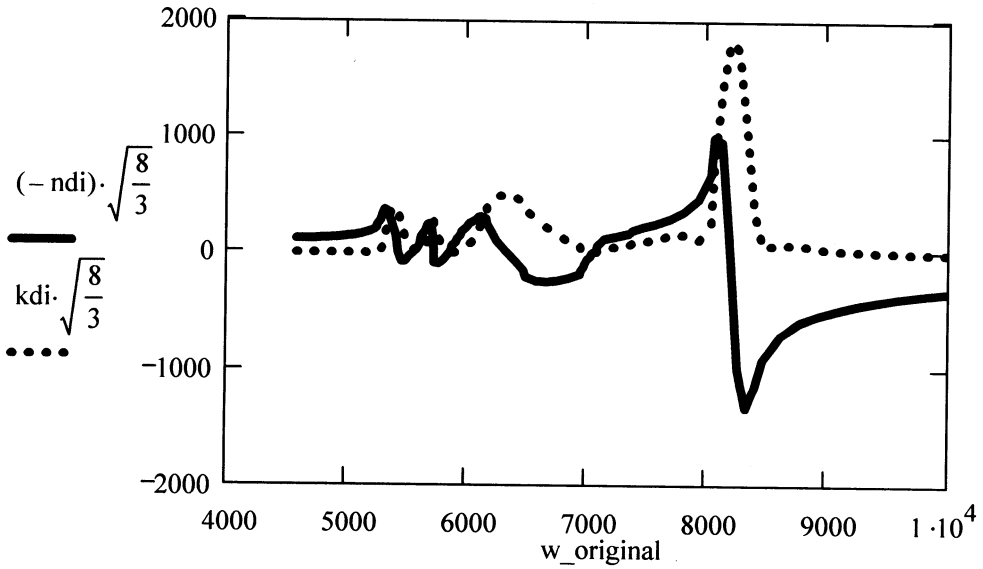

ndi_nubar := augment(ndi, w1)

$$\lambda 1 := \frac{10^7}{w1} \qquad i := 0..255$$

ndi_lambda := augment(ndi, λ1)

lambda_n_k_isa := augment(λ1, ndi)

lambda_n_k_isa := augment(lambda_n_k_isa, kdi)

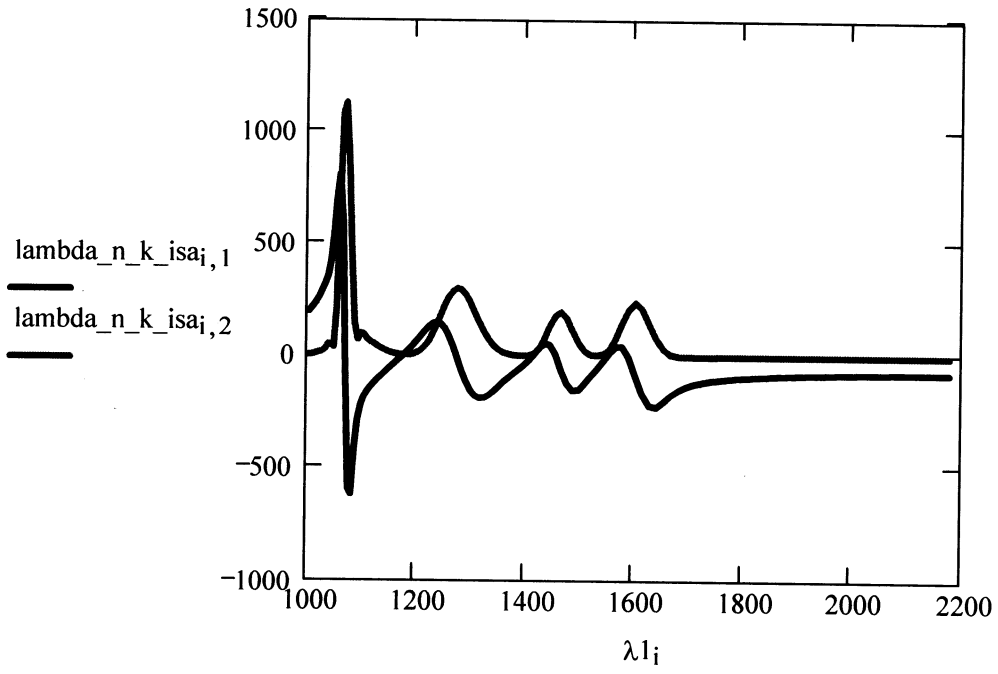

Final result: Absorbance data of isoamyl alcohol is transformed into refractive index spectra via Kramers-Kronig transformation.

APPENDIX B

FRESNEL CALCULATIONS OF ISOAMYL ALCOHOL (ISA)

Fresnel Calcs and Optical Const

This worksheet is used to complete the next steps in the experimental approach The first step is done in previous section: appendix A: Kramers-Kronig transformation of isoamyl alcohol (ISA).

2. Construct a function to return the complex refractive index of isoamyl alcohol

Wavenumber, n and k Au data in the NIR range from 1micron to 2.2micron

$n_2 := 1 \quad n_0 := 1.71 \quad d_1 := 500 \quad n_3 := 1.35$

Wavelength scan simulation: To do this, we need to have the complex refractive index for both the Au film and the ISA as a function of wavelength.

a. Import k(λ) and n(λ) of Isoamyl alcohol data from the kkt isoamyl alcoholworksheet.mcd.

NwISA :=

F:\..\w_ndi_kdi_treatedisa090404.xls

NAuCorn :=

C:\..\au_lambdan_k550_2300nmdata rht.xls

$n_{ISA} := \text{submatrix}(NwISA, 0, \text{rows}(NwISA) - 1, 1, 1)$

$k_{ISA} := \text{submatrix}(NwISA, 0, \text{rows}(NwISA) - 1, 2, 2)$

$v_{ISA} := \text{submatrix}(NwISA, 0, \text{rows}(NwISA) - 1, 0, 0)$

$N_{ISA}(v) := \text{linterp}(v_{ISA}, n_{ISA}, v) + i \cdot \text{linterp}(v_{ISA}, k_{ISA}, v)$

$i := 0..111$

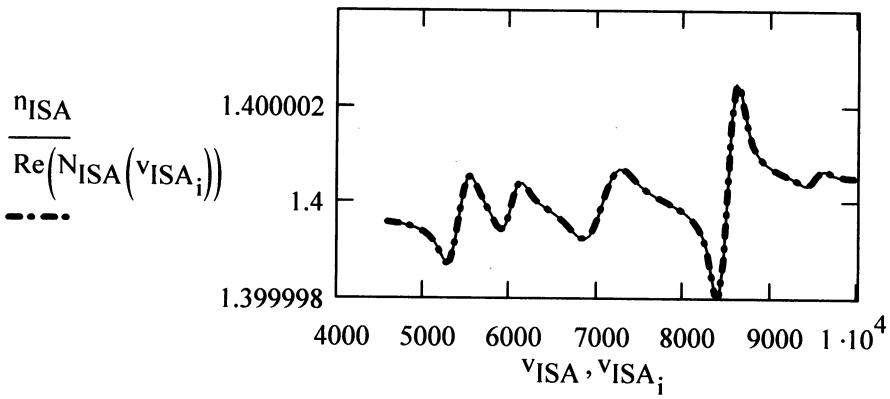

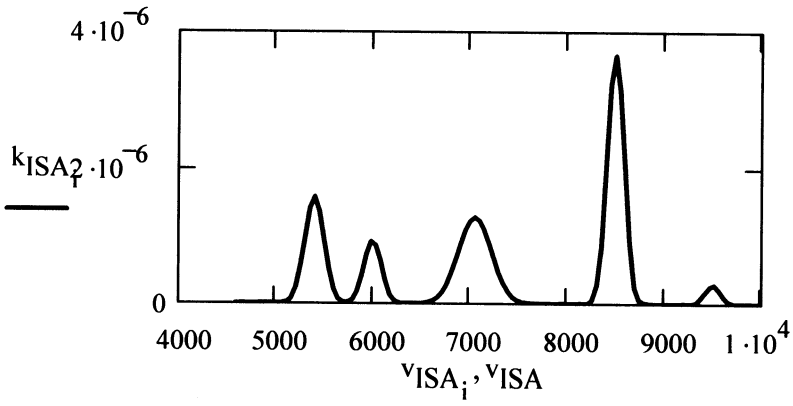

b. Complex refractive indicies of Au are also published by the Robert Corn research group, University of Wisconsin, Madison: http://corndog.chem.wisc.edu/fresnel/fcform.html

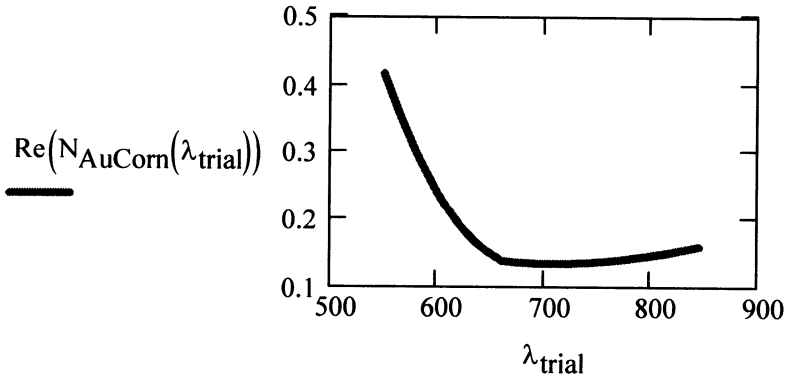

$\mathrm{Im}\left(N_{AuCorn}\left(\lambda_{trial}\right)\right)$

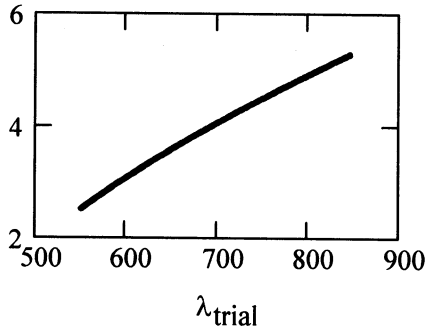

$\mathrm{Re}\left(N_{ISA}\left(\nu_{ISA_i}\right)\right)-1.4$

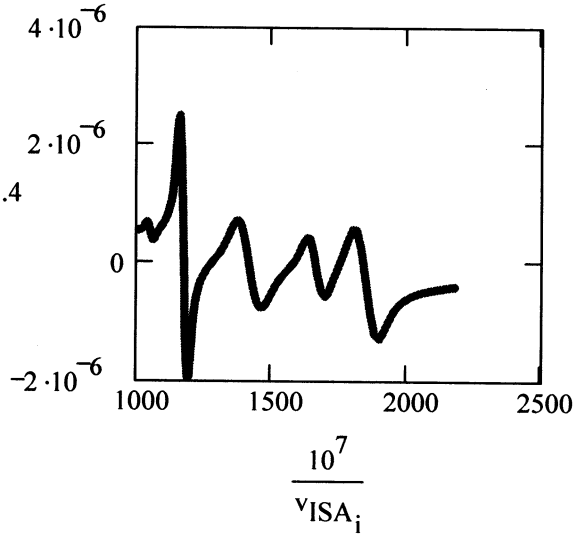

$\mathrm{Im}\left(N_{ISA}\left(\nu_{ISA_i}\right)\right)$

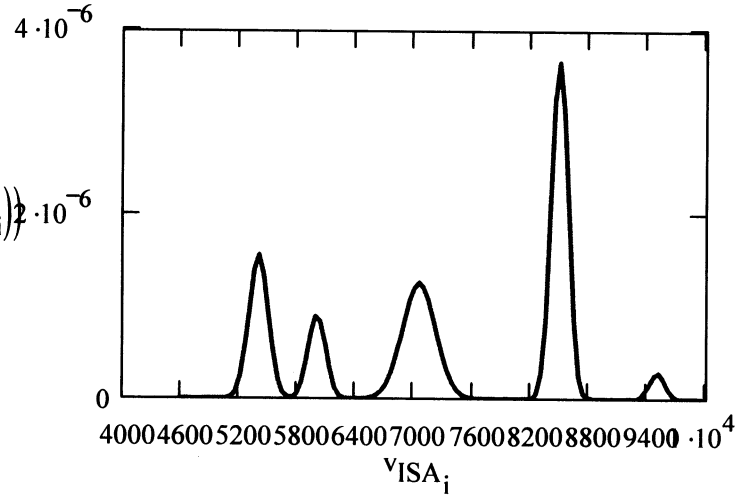

A function for producing n and k values from wavelength values

$$\lambda c(\upsilon) := \frac{1}{\upsilon} \cdot 10^8$$

A function to convert from wavenumbers to angstroms

$$\upsilon c(\lambda) := \frac{1}{\lambda} \cdot 10^8$$

3. Compute the theoretical reflectivity surface R(λ,θ) using the complex RI of ISA

a. Find the SPR angle of the fictious solvent at λ= 1500nm, n3 = 1.4

Fresnel equation is set to zero to find the SPR angle. Rp is the reflectivity, n refractive index, d thickness, θ angle, λ wavelength. There are four layers in this setup with subscripts in the following order: 0 is prism, 1 gold layer, 2 air, 3 isoamyl alcohol or fictious solvent

$$TOL := 0.0001$$

$$\theta := 55 \cdot \frac{\pi}{180}$$

Given

$$\left(\left| Rp\left(\theta, n_0, d_1, N_{AuCorn}(\lambda), 0, n_2, 1.4, \lambda \cdot 10\right) \right| \right)^2 = 0$$

n1 is complex refractive index of gold layer. d2 equals zero and n3 equals the refractive index of the fictious solvent.

$$\theta_{minSolvent}(\lambda) := MinErr(\theta) \cdot \frac{180}{\pi}$$

$$\theta_{minSolvent}(1102) = 56.631$$

b. Find the SPR angle of the isoamyl alcohol at λ= 1500nm, n3=N_ISA(λ)

$$\theta := 58 \cdot \frac{\pi}{180}$$

$$TOL := 0.0001$$

Given

$$\left(\left| Rp\left(\theta, n_0, d_1, N_{AuCorn}(\lambda), 0, n_2, N_{ISA}\left(\frac{10^7}{\lambda} \right), \lambda \cdot 10 \right) \right| \right)^2 = 0$$

n3 equals the complex refractive index of isoamyl alcohol.

$$\theta_{minISA}(\lambda) := MinErr(\theta) \cdot \frac{180}{\pi}$$

$$\theta_{minISA}(1102) = 56.631$$

4. Calculate the set of SPR angles from the theoretical reflectivity surface R(λ,θ) for a set of wavelengths

a. Dispersion curve for a fictious solvent layer 4 (n3=1.4)

$$TOL := 0.0001$$

$$jj := 0 .. 509$$

$$tt_{jj} := 1100 + 2 \cdot jj$$

$$\theta f_{solvent_{jj}} := \theta_{minSolvent}(tt_{jj})$$

b. Dispersion curve for isoamyl alcohol layer

$$TOL := 0.0001$$

$$jj := 0 .. 509 + 2 \cdot jj$$

$$\theta f_{ISA_{jj}} := \theta_{minISA}(tt_{jj}) \qquad \theta_{minISA}(1420) = 55.87$$

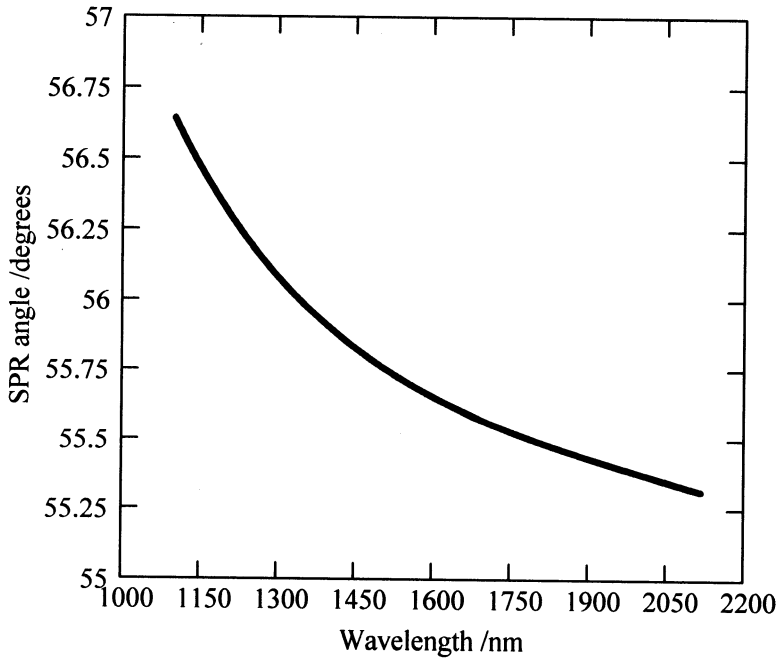

5. Construct a set of data corresponding to $\Delta\theta$_SPR(λ)

New delta_thetamin set without the bad data points.

$\Delta\theta min :=$

F:\..\w_delta_angle.xls

$wavelength := submatrix(\Delta\theta min, 0, rows(\Delta\theta min) - 1, 0, 0)$

$delta\theta min := submatrix(\Delta\theta min, 0, rows(\Delta\theta min) - 1, 1, 1)$

6. Compare Δθ_SPR(λ) to n(λ) spectrum of ISA

$$\frac{-\text{deltaθmin}}{\left(\text{Re}\left(N_{ISA}\left(v_{ISA_i}\right)\right)-1.4\right)\cdot 100}$$

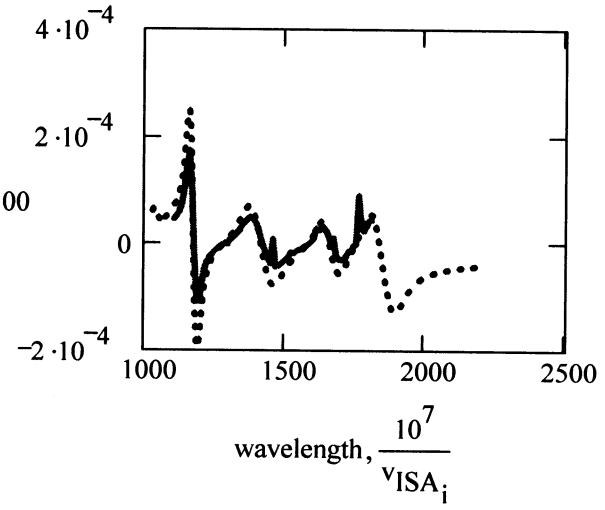

7. Construct a set of data corresponding to ΔR_SPR(λ)

Wavelength scan with n3 = 1.4 and n3 = N(ISA)

$ii := 0..73 \qquad jj := 0..509 \qquad tt_{jj} := 1100 + 2\cdot jj \qquad AA_{ii} := 52.8 + 0.2\cdot ii$

$$Fictious\_solvent_{jj,ii} := \left(\left|Rp\left(AA_{ii}\cdot\frac{\pi}{180}, n_0, d_1, N_{AuCorn}\left(tt_{jj}\right), 0, n_2, 1.4, tt_{jj}\cdot 10\right)\right|\right)^2$$

$$ISA_{jj,ii} := \left(\left|Rp\left(AA_{ii}\cdot\frac{\pi}{180}, n_0, d_1, N_{AuCorn}\left(tt_{jj}\right), 0, n_2, N_{ISA}\left(\frac{10^7}{tt_{jj}}\right), tt_{jj}\cdot 10\right)\right|\right)^2$$

$\Delta R\_SPR := Fictious\_solvent - ISA$

8. Compare ΔR_SPR(λ) to k(λ) spectrum of ISA

a. Reflectivity difference at an angle less than the SPR angle

ΔR(λ) for the series of angles starting at 52.8 degres with an increment of 0.2 degree. The range of angles of resonance is 55.3 - 55.6 degrees and the wavelength range is 1100 - 2120 nm.

Reflectivity difference at an angle $\theta < \theta\_SPR$

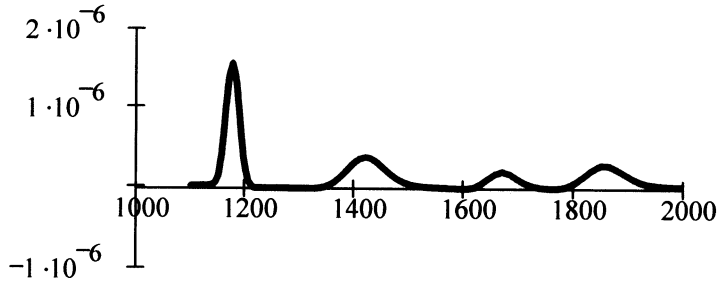

$\theta = 53$

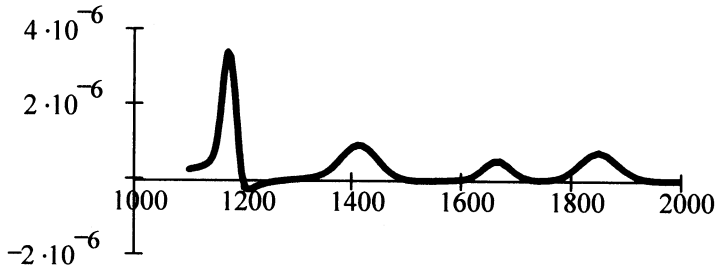

$\theta = 54$

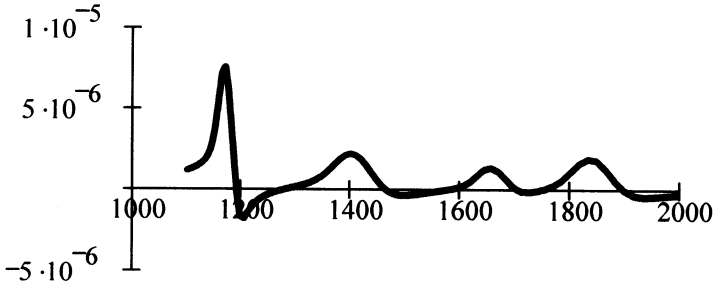

$\theta = 54.6$

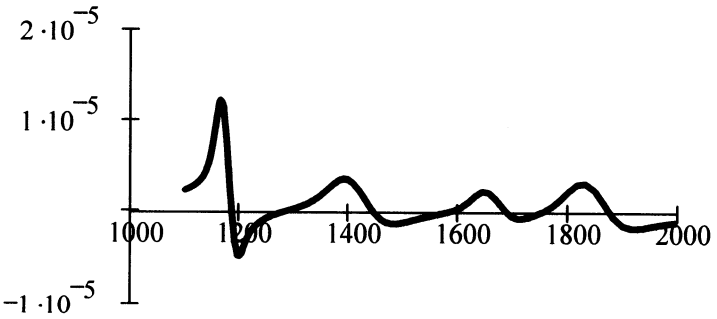

$\theta = 54.8$

b. Reflectivity difference at an angle equal the SPR angle

$\Delta R(\lambda)$ for the series of angles starting at 53 degres with an increment of 0.05 degree. The range of angles of resonance is 55.3 - 55.6 degrees and the wavelength range is 1100 - 2120 nm.

Wavelength scan with n3 = 1.4 and n3 = N(ISA)

$tt_{jj} := 1100 + 2 \cdot jj \qquad jj := 0 .. 509 \qquad aa_{ii} := 55 + 0.05 \cdot ii \qquad ii := 0 .. 73$

$$Fictious\_solvent_{jj,ii} := \left(\left| Rp\left(aa_{ii} \cdot \frac{\pi}{180}, n_0, d_1, N_{AuCorn}(tt_{jj}), 0, n_2, 1.4, tt_{jj} \cdot 10 \right) \right| \right)^2$$

$$ISA_{jj,ii} := \left(\left| Rp\left(aa_{ii} \cdot \frac{\pi}{180}, n_0, d_1, N_{AuCorn}(tt_{jj}), 0, n_2, N_{ISA}\left(\frac{10^7}{tt_{jj}} \right), tt_{jj} \cdot 10 \right) \right| \right)^2$$

$\Delta R\_SPR := Fictious\_solvent - ISA$

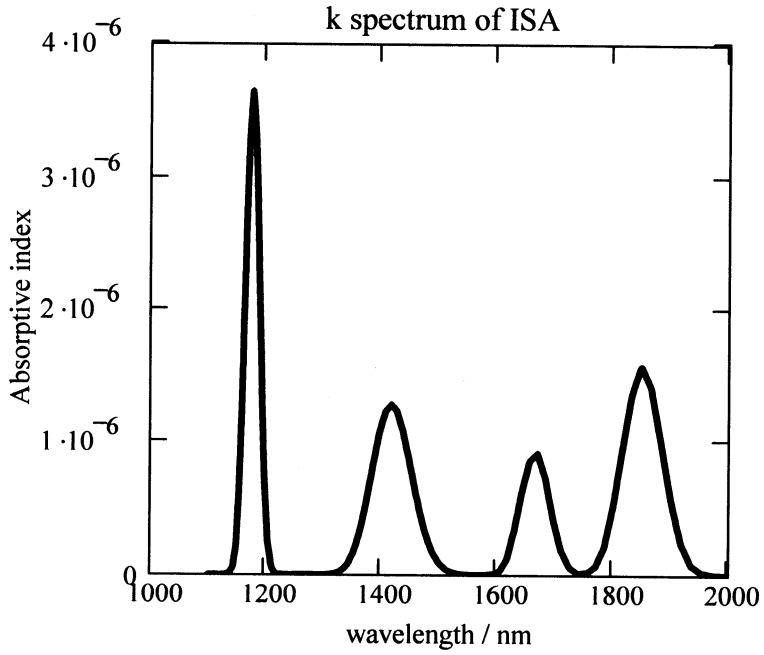

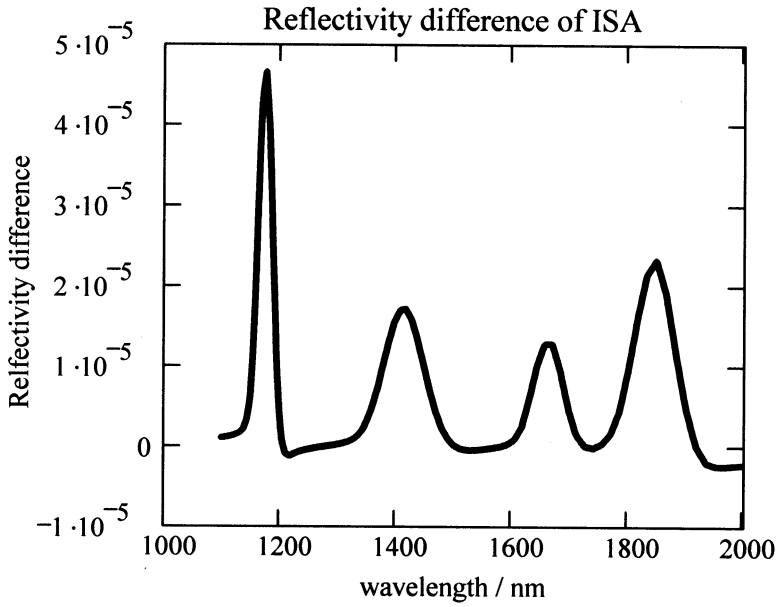
Reflectivity difference of ISA
Relfectivity difference
5 ·10^−5
4 ·10^−5
3 ·10^−5
2 ·10^−5
1 ·10^−5
0
−1 ·10^−5
1000
1200
1400
1600
1800
2000
wavelength / nm

Reflectivity difference at an angle θ ~θ _SPR

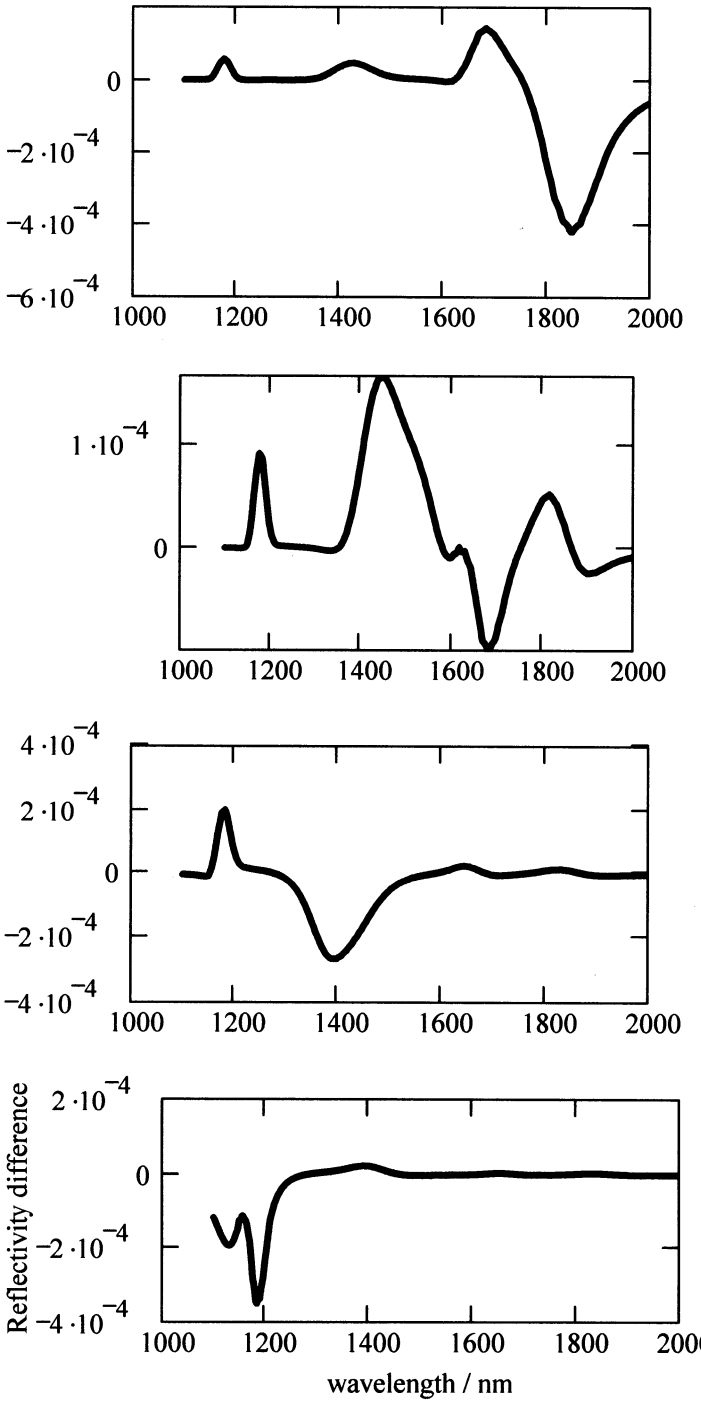

c. Reflectivity difference at an angle greater than the SPR angle

$\Delta R(\lambda)$ for the series of angles starting at 53 degres with an increment of 0.5 degree. The range of angles of resonance is 55.3 - 55.6 degrees and the wavelength range is 1100 - 2120 nm.

Wavelength scan with n3 = 1.4 and n3 = N(ISA)

$tt_{jj} := 1100 + 2 \cdot jj \qquad aa_{ii} := 57 + 0.5 \cdot ii$

$ii := 0 .. 73 \qquad jj := 0 .. 509$

$$Fictious\_solvent_{jj,ii} := \left(\left| Rp\left(aa_{ii} \cdot \frac{\pi}{180}, n_0, d_1, N_{AuCorn}(tt_{jj}), 0, n_2, 1.4, tt_{jj} \cdot 10 \right) \right| \right)^2$$

$$ISA_{jj,ii} := \left(\left| Rp\left(aa_{ii} \cdot \frac{\pi}{180}, n_0, d_1, N_{AuCorn}(tt_{jj}), 0, n_2, N_{ISA}\left(\frac{10^7}{tt_{jj}} \right), tt_{jj} \cdot 10 \right) \right| \right)^2$$

$\Delta R\_SPR := Fictious\_solvent - ISA$

Reflectivity difference at an angle θ > θ_SPR

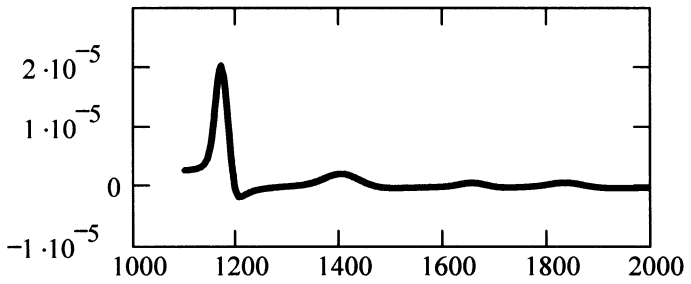

θ = 58

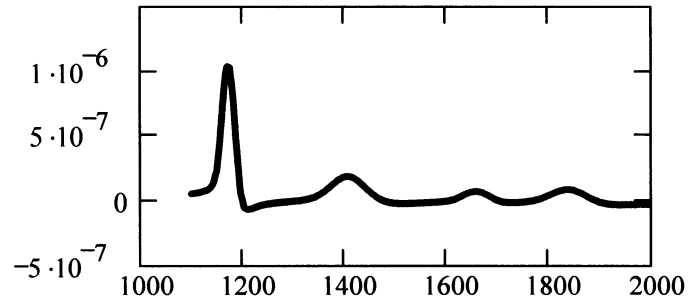

θ = 68

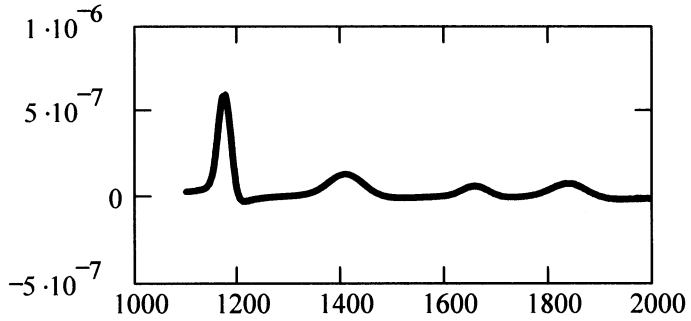

θ = 78

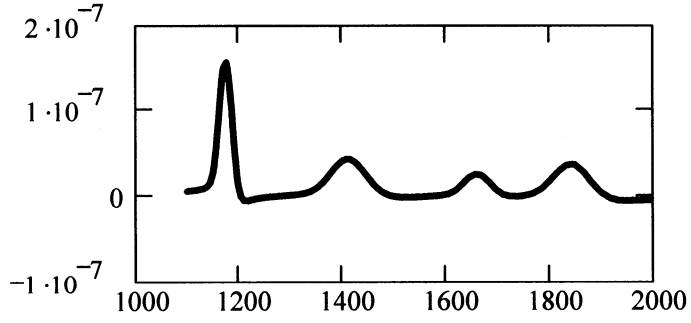

θ = 88

Illustrations of reflectivity in the conventional ATR spectroscopy and in the SPR-coupled ATR spectroscopy.

1. SPR-coupled ATR spectroscopy

$d_1 := 500 \qquad j := 0..299 \qquad \theta_j := \left(30 + \frac{j}{10}\right)\cdot\frac{\pi}{180} \qquad n_2 = 1$

$n_0 = 1.71 \qquad d_1 = 500 \qquad \lambda := 1500$

$Real1500_j := \left(\left|Rp\left(\theta_j, n_0, d_1, N_{AuCorn}(\lambda), 0, n_2, 1.4, \lambda\cdot 10\right)\right|\right)^2$

$Air_j := \left(\left|Rp\left(\theta_j, n_0, d_1, N_{AuCorn}(\lambda), 0, n_2, 1.00, \lambda\cdot 10\right)\right|\right)^2$

Coupling when layer 4 (n3) is 1.4 (isoamyl alcohol, real part) and 1.00 (air)

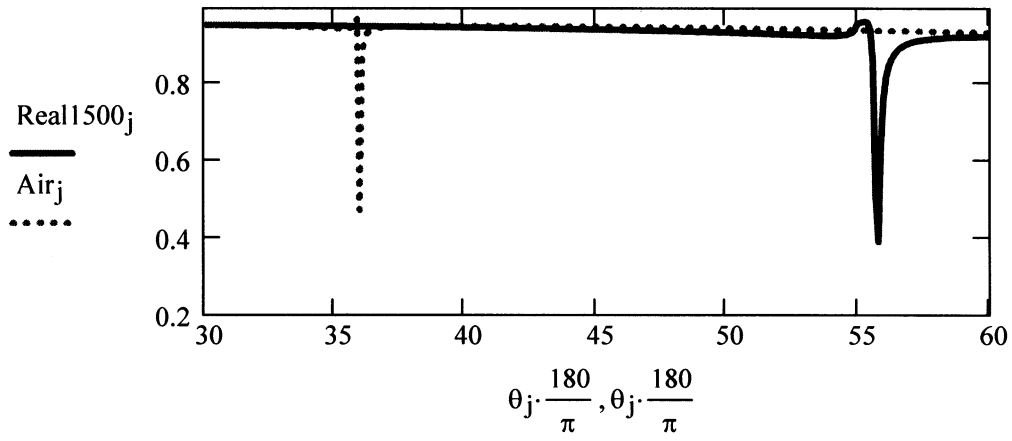

2. Conventional ATR spectroscopy

$\theta_j := \left(30 + \frac{j}{10}\right)\cdot\frac{\pi}{180} \qquad j := 0..299 \qquad d_1 := 0 \qquad n_0 = 1.71$

$\lambda := 1500 \qquad n_2 = 1$

$RReal1500_j := \left(\left|Rp\left(\theta_j, n_0, d_1, N_{AuCorn}(\lambda), 0, n_2, 1.4, \lambda\cdot 10\right)\right|\right)^2$

$$AAir_j := \left(\left| Rp\left(\theta_j, n_0, d_1, N_{AuCorn}(\lambda), 0, n_2, 1.00, \lambda \cdot 10\right) \right| \right)^2$$

Coupling when layer 4 (n3) is 1.4 (isoamyl alcohol, real part) and 1.00 (air).

This plot just illustrates the reflectivity in the conventional ATR where there is no SPW coupling to cause a dip in reflectivity.